Multicomponent compact Abelian-Higgs lattice models

Andrea Pelissetto
Dipartimento di Fisica dell'Università di Roma Sapienza and INFN Sezione di Roma I, I-00185 Rome, Italy

Ettore Vicari
Dipartimento di Fisica dell'Università di Pisa and INFN Largo Pontecorvo 3, I-56127 Pisa, Italy

(Received 13 September 2019; published 25 October 2019)

We investigate the phase diagram and critical behavior of three-dimensional multicomponent Abelian-Higgs models, in which an N-component complex field $z_{\boldsymbol{x}}^a$ of unit length and charge is coupled to compact quantum electrodynamics in the usual Wilson lattice formulation. We determine the phase diagram and study the nature of the transition line for $N = 2$ and $N = 4$. Two phases are identified, specified by the behavior of the gauge-invariant local composite operator $Q_{\boldsymbol{x}}^{ab} = \bar{z}_{\boldsymbol{x}}^a z_{\boldsymbol{x}}^b - \delta^{ab}/N$, which plays the role of order parameter. In one phase, we have $\langle Q_{\boldsymbol{x}}^{ab} \rangle = 0$, while in the other $Q_{\boldsymbol{x}}^{ab}$ condenses. Gauge correlations are never critical: gauge excitations are massive for any finite coupling. The two phases are separated by a transition line. Our numerical data are consistent with the simple scenario in which the nature of the transition is independent of the gauge coupling. Therefore, for any finite positive value of the gauge coupling, we predict a continuous transition in the Heisenberg universality class for $N = 2$ and a first-order transition for $N = 4$. However, notable crossover phenomena emerge for large gauge couplings, when gauge fluctuations are suppressed. Such crossover phenomena are related to the unstable O($2N$) fixed point, describing the behavior of the model in the infinite gauge-coupling limit.

DOI: 10.1103/PhysRevE.100.042134

I. INTRODUCTION

Models of complex scalar matter fields coupled to gauge fields have been much studied in condensed matter physics, since they are believed to describe several interesting systems, such as superconductors and superfluids, quantum Hall states, quantum SU(N) antiferromagnets, unconventional quantum phase transitions, etc.; see, e.g., Refs. [1–6] and references therein. Scalar electrodynamics, or Abelian-Higgs (AH) model, is a paradigmatic model, in which an N-component complex scalar field $\boldsymbol{\Phi}$ is minimally coupled to the electromagnetic field A_μ. The corresponding continuum Lagrangian reads

$$\mathcal{L} = |D_\mu \boldsymbol{\Phi}|^2 + r\,|\boldsymbol{\Phi}|^2 + \frac{1}{6} u\,(|\boldsymbol{\Phi}|^2)^2 + \frac{1}{4g^2} F_{\mu\nu}^2, \qquad (1)$$

where $F_{\mu\nu} \equiv \partial_\mu A_\nu - \partial_\nu A_\mu$, and $D_\mu \equiv \partial_\mu + i A_\mu$. The renormalization-group (RG) analysis of the continuum AH model [7,8] should provide information on the nature of the finite-temperature phase transitions occurring in d-dimensional systems characterized by a global SU(N) symmetry and a local U(1) gauge symmetry.

In this paper we consider the multicomponent AH model, in which the scalar field $\boldsymbol{\Phi}$ has $N \geqslant 2$ components. Such a model has a local U(1) gauge invariance and a global SU(N) invariance. We assume that the field belongs to the fundamental representation of the U(1) group, i.e., it has charge 1. The one-component AH model has been extensively discussed in the literature [9–13]. In three dimensions, these systems may undergo continuous transitions in the XY universality class.

Lattice formulations of the three-dimensional AH model are obtained by associating complex N-component unit vectors $z_{\boldsymbol{x}}$ with the sites $\boldsymbol{x}$ of a cubic lattice, and U(1) variables $\lambda_{\boldsymbol{x},\mu}$ with each link connecting the site $\boldsymbol{x}$ with the site $\boldsymbol{x} + \hat{\mu}$ (where $\hat{\mu} = \hat{1}, \hat{2}, \ldots$ are unit vectors along the lattice directions). The partition function of the system reads

$$Z = \sum_{\{z\},\{\lambda\}} e^{-H}, \qquad (2)$$

where the Hamiltonian is [14]

$$H = -\beta N \sum_{\boldsymbol{x},\mu} (\bar{z}_{\boldsymbol{x}} \cdot \lambda_{\boldsymbol{x},\mu}\, z_{\boldsymbol{x}+\hat{\mu}} + \text{c.c.}) - \beta_g \sum_{\boldsymbol{x},\mu>\nu} (\lambda_{\boldsymbol{x},\mu}\, \lambda_{\boldsymbol{x}+\hat{\mu},\nu}\, \bar{\lambda}_{\boldsymbol{x}+\hat{\nu},\mu}\, \bar{\lambda}_{\boldsymbol{x},\nu} + \text{c.c.}); \qquad (3)$$

the first sum runs over all lattice links, while the second one runs over all plaquettes.

For $\beta_g = 0$ we recover a particular lattice formulation of the CP^{N-1} model, which is quadratic with respect to the spin variables and contains explicit gauge link variables. The CP^{N-1} model has been extensively studied. In spite of several field-theoretical and numerical studies for $N = 2, 3, 4$ and $N \to \infty$, there are still some controversies on the nature of its transition [6,8,15–19]. For $\beta_g \to \infty$ the gauge link variables are all equal to 1 modulo gauge transformations and the AH model becomes equivalent to the standard O(n) vector model with $n = 2N$, whose critical behavior is well understood [20]. We also mention that some numerical results for the AH lattice

model (3) have been reported in Refs. [6,21,22], but a definite picture has not been achieved yet [23].

It is important to stress that we consider the lattice compact version of electrodynamics (the so-called Wilson lattice formulation of gauge theories). In the absence of matter fields, its behavior [24] is controlled by topological excitations, the monopoles, which are instead suppressed in noncompact formulations. Therefore, the critical properties of the AH lattice model that we consider might differ from those of the model in which gauge fields are noncompact.

In this paper we investigate the phase diagram and the nature of the phase transitions of the three-dimensional AH model (3). We consider systems with $N = 2$ and $N = 4$, and investigate the nature of the transition line by varying β at fixed gauge coupling β_g, for some values of β_g. In both cases the phase diagram of the AH lattice model (3) turns out to present two phases: for small β there is a disordered confined phase, while for large values of β there is an ordered phase in which correlations of the gauge-invariant Hermitian operator $Q^{ab}_{\boldsymbol{x}} = \bar{z}^a_{\boldsymbol{x}} z^b_{\boldsymbol{x}} - \delta^{ab}/N$ show long-range order. In both phases, and also along the transition line, the correlations of gauge variables do not show a critical behavior. The gauge coupling β_g does not play any significant role: the features of two phases are the same for any finite β_g. The two phases are separated by a single transition line, which connects the CP^{N-1} transition point ($\beta_g = 0$) to the O($2N$) transition point ($\beta_g = \infty$) in the space of the two parameters β and β_g. For $\beta_g = 0$ the transition is continuous for $N = 2$ (belonging to the Heisenberg universality class) and of first order for $N = 4$. We conjecture that the nature of the transitions along the line separating the ordered and disordered phases does not change with β_g. Therefore, the transition is always continuous (discontinuous) for $N = 2$ ($N = 4$). We also observe significant deviations for β_g large ($\beta_g \gtrsim 1$), i.e., when gauge fluctuations are suppressed. They are interpreted as a crossover phenomenon due to the presence of an O($2N$) vector transition in the limit $\beta_g \to \infty$.

The paper is organized as follows. In Sec. II we review the field-theoretical results for the AH model. In Sec. II A we review the ε-expansion predictions obtained in the continuum AH model, and in Sec. II B we present instead the results of the Landau-Ginzburg-Wilson (LGW) approach based on a gauge-invariant order parameter. The two approaches are critically compared in Sec. II C. The numerical results are presented in Sec. III. The definitions of the quantities we consider are given in Sec. III A, while Secs. III B and III C present our results for $N = 2$ and 4, respectively, focusing on the behavior of the gauge-invariant order parameter. Results for vector and gauge observables are presented in Sec. III D. In Sec. IV we summarize and present our conclusions. In Appendix A we present some results for tensor correlations in n-vector models. In Appendix B we discuss the limit $\beta_g \to \infty$.

II. FIELD THEORETICAL APPROACHES

In this section we outline some apparently alternative field-theoretical approaches which can be employed to infer the nature of the phase transitions in systems characterized by a U(N) global symmetry and a local U(1) gauge symmetry, such as the AH lattice model.

A. Renormalization-group flow in the AH model close to four dimensions

We now summarize the main features of the RG flow in the continuum AH model (1), which has been analyzed close to four dimensions in the $\varepsilon \equiv 4 - d$ expansion framework [7,25,26], using the functional RG approach [27], and in the large-N limit [8].

Close to four dimensions, the RG flow in the space of the renormalized couplings u and $f \equiv g^2$ [we rescale them as $u \to u/(24\pi^2)$ and $f \to f/(24\pi^2)$ to simplify the equations] can be computed in perturbation theory. At one loop, the β functions read [7]

$$\beta_u \equiv \mu \frac{\partial u}{\partial \mu} = -\varepsilon u + (N+4)u^2 - 18uf + 54f^2,$$
$$\beta_f \equiv \mu \frac{\partial f}{\partial \mu} = -\varepsilon f + Nf^2. \tag{4}$$

One can easily verify that a stable fixed point exists only for $N > N_c(\varepsilon)$, with

$$N_c(\varepsilon) = N_4 + O(\varepsilon), \quad N_4 = 90 + 24\sqrt{15} \approx 183. \tag{5}$$

The corresponding zero of the β functions is

$$f^* = \frac{\varepsilon}{N}, \tag{6}$$

$$u^* = \frac{N + 18 + \sqrt{N^2 - 180N - 540}}{2N(N+4)}\,\varepsilon \approx \frac{\varepsilon}{N}. \tag{7}$$

The presence of a stable fixed point indicates that these systems may undergo a continuous transition if N is large enough [$N > N_c(1)$ in three dimensions], in agreement with the direct large-N analysis [8]. The qualitative picture obtained in the one-loop calculation is not changed by higher-order calculations. The perturbative expansion has been recently extended to four loops [25], obtaining $N_c(\varepsilon)$ to $O(\varepsilon^3)$,

$$N_c(\varepsilon) = N_4[1 - 1.752\,\varepsilon + 0.789\,\varepsilon^2 + 0.362\,\varepsilon^3 + O(\varepsilon^4)]. \tag{8}$$

The large coefficients make a reliable three-dimensional ($\varepsilon = 1$) estimate quite problematic. Nevertheless, by means of a resummation of the expansion, Ref. [25] obtained the estimate $N_c = 12.2(3.9)$ in three dimensions, which confirms the absence of a stable fixed point for small values of N.

In the limit $\beta_g \to \infty$, the lattice AH model (3) is equivalent to the symmetric O($2N$) vector theory. Therefore, for large β_g one expects significant crossover effects, which increase as β_g increases, due to the nearby O($2N$) critical behavior. In the continuum AH model, the crossover is controlled by the RG flow in the vicinity of the O($2N$) fixed point

$$u^*_{\mathrm{O}(2N)} = \frac{1}{N+4}\varepsilon, \quad f = 0. \tag{9}$$

This fixed point exists for any N and is always unstable. The analysis of the stability matrix $\Omega_{ij} = \partial\beta_i/\partial g_j$ shows that it has a positive eigenvalue $\lambda_u = \omega$, where $\omega > 0$ is the exponent controlling the leading scaling corrections in O($2N$) vector models [20], and a negative eigenvalue, which gives the

dimension of the operator that controls the crossover behavior,

$$\lambda_f = \left.\frac{\partial \beta_f}{\partial f}\right|_{f=0,u=u^*}. \tag{10}$$

Since the β function $\beta_f(u, f)$ associated with f has the general form

$$\beta_f = -\varepsilon f + f^2 F(u, f), \tag{11}$$

where $F(u, f)$ has a regular perturbative expansion (see, e.g., the four-loop expansion reported in Ref. [25]), we obtain

$$\lambda_f = -\varepsilon \tag{12}$$

to all orders in perturbation theory. Therefore, the crossover exponent $y_f = -\lambda_f$ is 1 in three dimensions. Note that these crossover features related to the unstable O($2N$) fixed point are independent of the existence of the stable fixed point, which is only relevant to predict the eventual asymptotic behavior.

B. Gauge-invariant Landau-Ginzburg-Wilson framework

An alternative field-theoretical approach is the LGW framework [15,20,28–31], in which one assumes that the relevant critical modes are associated with the gauge-invariant local composite site variable

$$Q_{\boldsymbol{x}}^{ab} = \bar{z}_{\boldsymbol{x}}^a z_{\boldsymbol{x}}^b - \frac{1}{N}\delta^{ab}, \tag{13}$$

which is a Hermitian and traceless $N \times N$ matrix. As discussed in Refs. [15,19,32], this is a highly nontrivial assumption, as it postulates that gauge fields do not play a relevant role in the effective theory. The order-parameter field in the corresponding LGW theory is therefore a traceless Hermitian matrix field $\Psi^{ab}(\boldsymbol{x})$, which can be formally defined as the average of $Q_{\boldsymbol{x}}^{ab}$ over a large but finite lattice domain. The LGW field theory is obtained by considering the most general fourth-order polynomial in Ψ consistent with the U(N) global symmetry:

$$\begin{aligned}\mathcal{H}_{\rm LGW} = {} & \mathrm{Tr}(\partial_\mu \Psi)^2 + r\,\mathrm{Tr}\,\Psi^2 \\ & + w\,\mathrm{tr}\,\Psi^3 + u\,(\mathrm{Tr}\,\Psi^2)^2 + v\,\mathrm{Tr}\,\Psi^4.\end{aligned} \tag{14}$$

Also in this framework continuous transitions may only arise if the RG flow in the LGW theory has a stable fixed point.

For $N = 2$, the cubic term in Eq. (14) vanishes and the two quartic terms are equivalent. Therefore, one recovers the O(3)-symmetric vector LGW theory, leading to the prediction that the phase transition may be continuous and, in this case, that it belongs to the Heisenberg universality class. For $N \geqslant 3$, the cubic term is generally expected to be present. Its presence is usually taken as an indication that phase transitions occurring in this class of systems are generally of first order. Indeed, a straightforward mean-field analysis shows that the transition is of first order in four dimensions where mean field applies. If statistical fluctuations are small—this is the basic assumption—the transition should be of first order also in three dimensions. In this scenario, continuous transitions may still occur, but they require a fine tuning of the microscopic parameters leading to the effective cancellation of the cubic term. These arguments were originally [15,18] applied to predict the behavior of CP^{N-1} models. However, as they are only based on symmetry considerations, they can be extended to AH lattice models, as well.

C. Comparison of the alternative field-theoretical approaches

The two field-theoretical approaches outlined above give inconsistent predictions both for small and large values of N. The contradiction is quite striking for the two-component $N = 2$ case. For this value of N, the continuum AH model predicts the absence of continuous transitions, due to the absence of a stable fixed point. On the other hand, a stable fixed point—it is the usual Heisenberg O(3) fixed point—exists in the effective LGW theory based on a gauge-invariant order parameter, leaving open the possibility of observing continuous transitions (first-order transitions are never excluded as the statistical model may be outside the attraction domain of the fixed point). The numerical results for the CP^1 lattice models [15,16], as well as the AH lattice results we shall present below, confirm the existence of continuous transitions in models with $N = 2$: the LGW theory provides the correct description of the large-scale behavior of these systems. There are at least two possible explanations for the failure of the continuum AH model. A first possibility is that it does not encode the relevant degrees of freedom at the transition. A second possibility is that the problem is not in the continuum AH model, but rather in the perturbative treatment around four dimensions. The three-dimensional fixed point may not be analytically related to a four-dimensional fixed point, and therefore it escapes any perturbative analysis in powers of ε.

We also recall that the perturbative AH approach of Sec. II A also fails for $N = 1$. Although no stable fixed point is identified in the ε expansion (see Sec. II A), these models may undergo continuous transitions in the XY universality class [9–11]. It is worth mentioning that there are also other systems in which the ε expansion fails to provide the correct physical picture in three dimensions. We mention the ϕ^4 theories describing frustrated spin models with noncollinear order [33,34] and the ^{3}He superfluid transition from the normal to the planar phase [35].

For large values of N, the continuum AH theory and the effective LGW approach give again contradictory results. Indeed, the former approach indicates that continuous transitions are possible, a prediction which is supported by the large-N analysis of lattice models; see, e.g., Ref. [15]. If one trusts the argument based on the relevance of the cubic term, the LGW approach predicts instead a first-order transition, unless a fine tuning of the microscopic parameters is performed. Again, there are two possible explanations for the different conclusions obtained in the LGW approach. A first possibility is that the critical modes at the transition are not exclusively associated with the gauge-invariant order parameter Q defined in Eq. (13). Other features, for instance the gauge degrees of freedom, may become relevant, requiring an effective description different from that of the LGW theory (14). If this interpretation is correct, the continuum AH model would be the correct theory as it includes the gauge fields explicitly. A second possibility is that the presence of a cubic term in the LGW Hamiltonian does not necessarily imply the absence of continuous transitions in three dimensions, as it is

usually assumed. It might be that statistical fluctuations soften the transition as one moves from four to three dimensions; see, e.g., Refs. [16,17] for a discussion of this issue.

While the two field-theoretical approaches give different predictions for $N = 1, 2$ and N large (more precisely, for $N > N_c$; see Sec. II A), for $3 \leqslant N < N_c$ they both predict that all models undergo a first-order transition. For $N = 3$ simulation results do not presently confirm it. Indeed, while numerical results for the lattice model with Hamiltonian (3) and $\beta_g = 0$ show a robust indication that the transition is of first order [15], the results for the loop model considered in Refs. [16,17] apparently favor a continuous transition. The available numerical results for lattice CP^3 models, i.e., for $N = 4$, are generally consistent with first-order transitions [6,15,17]. We also mention that Ref. [6] claims that the AH lattice model (3) undergoes a continuous transition for $\beta_g = 1$ and $N = 4$, a result which is at odds with the above arguments. However, as we shall show, the numerical results that we present later do not confirm their conclusions, but are instead consistent with a relatively weak first-order transition.

III. NUMERICAL RESULTS

A. Numerical simulations and observables

In this section we present a finite-size scaling (FSS) analysis of numerical results of Monte Carlo (MC) simulations for $N = 2$ and $N = 4$. For this purpose we consider cubic lattices of linear size L with periodic boundary conditions. We study the behavior of the system as a function of β at fixed β_g.

The linearity of Hamiltonian (3) with respect to each lattice variable allows us to employ an overrelaxed algorithm for the updating of the lattice configurations. It consists in a stochastic mixing of microcanonical and standard Metropolis updates of the lattice variables [36–38]. To update each lattice variable, we randomly choose either a standard Metropolis update, which ensures ergodicity, or a microcanonical move, which is more efficient than the Metropolis one but does not change the energy. On average, we perform three or four microcanonical updates for every Metropolis proposal. In the Metropolis update, changes are tuned so that the acceptance is 1/3.

We compute the energy density and the specific heat, defined as

$$E = \frac{1}{NV}\langle H\rangle, \quad C = \frac{1}{N^2V}(\langle H^2\rangle - \langle H\rangle^2), \tag{15}$$

where $V = L^3$. We consider correlations of the Hermitean gauge invariant operator (13). Its two-point correlation function is defined as

$$G(\boldsymbol{x}-\boldsymbol{y}) = \langle \mathrm{Tr}\, Q_x Q_y\rangle, \tag{16}$$

where the translation invariance of the system has been taken into account. The susceptibility and the correlation length are defined as $\chi = \sum_{\boldsymbol{x}} G(\boldsymbol{x})$ and

$$\xi^2 \equiv \frac{1}{4\sin^2(\pi/L)}\frac{\widetilde{G}(\boldsymbol{0}) - \widetilde{G}(\boldsymbol{p}_m)}{\widetilde{G}(\boldsymbol{p}_m)}, \tag{17}$$

where $\widetilde{G}(\boldsymbol{p}) = \sum_{\boldsymbol{x}} e^{i\boldsymbol{p}\cdot\boldsymbol{x}} G(\boldsymbol{x})$ is the Fourier transform of $G(\boldsymbol{x})$, and $\boldsymbol{p}_m = (2\pi/L, 0, 0)$ is the minimum nonzero lattice momentum. We also consider the Binder parameter

$$U = \frac{\langle \mu_2^2\rangle}{\langle \mu_2\rangle^2}, \quad \mu_2 = \sum_{\boldsymbol{x},\boldsymbol{y}} \mathrm{Tr}\, Q_{\boldsymbol{x}} Q_{\boldsymbol{y}}. \tag{18}$$

We consider correlations of the fundamental variable z_x. To obtain a gauge-invariant quantity, we consider correlations with λ strings, i.e., averages like

$$\mathrm{Re}\left\langle \bar{z}_{\boldsymbol{x}} \cdot z_{\boldsymbol{y}} \prod_{\ell\in\mathcal{C}} \lambda_\ell \right\rangle, \tag{19}$$

where the product extends over the link variables that belong to a lattice path $\mathcal{C}$ connecting points $\boldsymbol{x}$ and $\boldsymbol{y}$. To define quantities that have the correct FSS, the path $\mathcal{C}$ must be chosen appropriately, as discussed in Ref. [39]. Here, to simplify the calculations, we only consider correlations between points that belong to lattice straight lines. We define

$$G_V(d, L) = \frac{1}{V}\sum_{\boldsymbol{x}} \mathrm{Re}\left\langle \bar{z}_{\boldsymbol{x}} \cdot z_{\boldsymbol{x}+d\hat{\mu}} \prod_{n=0}^{d-1} \lambda_{\boldsymbol{x}+n\hat{\mu},\mu} \right\rangle, \tag{20}$$

where all coordinates should be taken modulo L because of the periodic boundary conditions. Note that in the definition of G_V we average over all lattice sites $\boldsymbol{x}$ exploiting the translation invariance of systems with periodic boundary conditions, and select a generic lattice direction $\hat{\mu}$ (in our MC simulations we also average over the three equivalent directions). Note also that $G_V(0, L) = 1$ and that $G_V(L, L)$ is the average value $P(L)$ of the Polyakov loop,

$$P(L) = \frac{1}{V}\sum_{\boldsymbol{x}} \mathrm{Re}\left\langle \prod_{n=0}^{L-1} \lambda_{\boldsymbol{x}+n\hat{\mu},\mu} \right\rangle. \tag{21}$$

Finally, we consider the so-called Wilson loop defined as

$$W(m, L) = \mathrm{Re}\left\langle \prod_{\ell\in\mathcal{C}} \lambda_\ell \right\rangle, \tag{22}$$

where the path $\mathcal{C}$ is a square of linear size m.

In the following we present a FSS analysis of the above observables, for $N = 2$ and $N = 4$ and some values of $\beta_g > 0$. In Fig. 1 we anticipate the resulting phase diagrams. For both $N = 2$ and 4, β_c decreases as β_g increases and, eventually, it converges to the value appropriate for the n-vector model with $n = 4$ and 8, $\beta_c = 0.233965(2)$ [40,41] and $\beta_c = 0.24084(1)$ [18].

As we shall discuss, our numerical data are consistent with a simple scenario in which the nature of the transitions along the line separating the ordered and disordered phases is unchanged for any finite $\beta_g \geqslant 0$. Therefore, for $N = 2$ the phase transitions are continuous and belong to the Heisenberg universality class as it occurs in the CP^1 model. The O(4) critical behavior occurs only for β_g strictly equal to ∞. For $N = 4$ instead, transitions are of first order, except for $\beta_g = \infty$, where the system develops an O(8) vector critical behavior.

B. Continuous transitions for $N = 2$

As already mentioned, lattice versions of the three-dimensional CP^1 model undergo continuous transitions

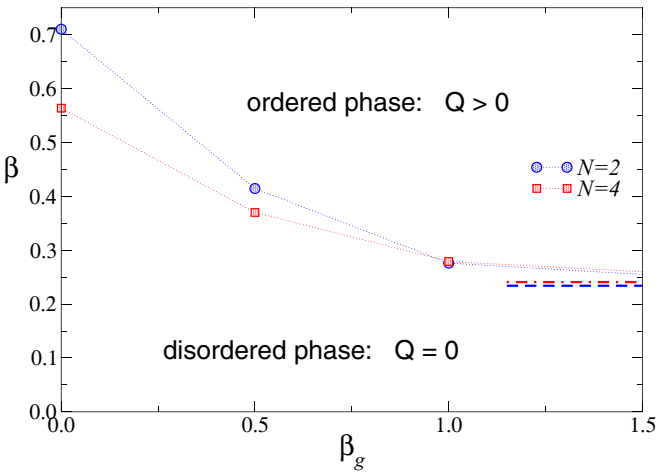

FIG. 1. The phase diagram of the AH lattice model in the space of parameters β and β_g, for $N = 2$ and $N = 4$. The points are the MC estimates of the critical points; the dotted lines that connect them are meant only to guide the eye. The horizontal lines indicate the limiting values of β_c for $\beta_g \to \infty$ for $N = 2$ ($\beta_c \approx 0.23396$, dashed) and $N = 4$ ($\beta_c \approx 0.24084$, dot-dashed): they correspond to the critical β_c for the standard three-dimensional O(4) and O(8) vector models, respectively. For $\beta_g = 0$, we have [15] $\beta_c = 0.7102(1)$ ($N = 2$) and $\beta_c = 0.5636(1)$ ($N = 4$).

belonging to the Heisenberg universality class, i.e., to that of the standard $N = 3$ vector model. This has been also shown [15] for model (3) with $\beta_g = 0$ [$\beta_c = 0.7102(1)$ in this case]. On the other hand, for $\beta_g = \infty$ the model is equivalent to the standard O(4) vector model that has a continuous transition for [40,41] $\beta_c = 0.233965(2)$. As already inferred from the RG flow of the AH continuum theory, the $\beta_g = \infty$ O(4) critical behavior is expected to be unstable against perturbations associated with nonzero values of β_g^{-1}. Therefore, the most natural hypothesis is that the all transitions for finite $\beta_g \geqslant 0$ belong to the Heisenberg universality class. However, a substantial crossover from the O(4) to the O(3) behavior is expected to characterize the transition for relatively large values of β_g, $\beta_g \gtrsim 1$ say.

To provide evidence of this scenario, we perform MC simulations for $\beta_g = 0.5$ and 1. As in our previous work [15], we study the FSS behavior of the Binder parameter U and of $R_\xi = \xi/L$. At continuous transitions the FSS limit is obtained by taking $\beta \to \beta_c$ and $L \to \infty$ keeping

$$X \equiv (\beta - \beta_c) L^{1/\nu} \tag{23}$$

fixed. Any RG invariant quantity R, such as $R_\xi \equiv \xi/L$ and U, is expected to asymptotically behave as

$$R(\beta, L) = f_R(X) + O(L^{-\omega}), \tag{24}$$

where $\omega > 0$ is the leading scaling correction exponent [20], and $f_R(X)$ is universal apart from a normalization of its argument. The function $f_R(X)$ only depends on the shape of the lattice and on the boundary conditions. In the case of the Heisenberg universality we have [20,42–44] $\nu = 0.7117(5)$ and $\omega = 0.78(1)$. As R_ξ is monotonically increasing as a function of X, Eq. (24) implies that

$$U = F(R_\xi) + O(L^{-\omega}), \tag{25}$$

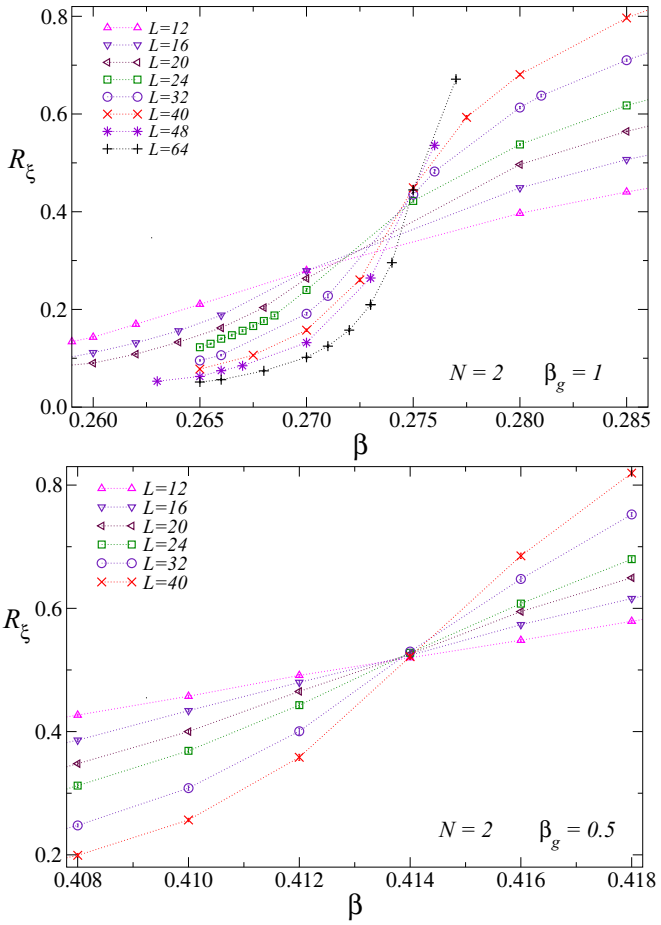

FIG. 2. R_ξ versus β in the $N = 2$ AH lattice model, for $\beta_g = 0.5$ (bottom) and $\beta_g = 1$ (top). In both cases the data for different values of L show a crossing point, whose position provides an estimate of the critical point: $\beta_c = 0.4145(5)$ and $\beta_c = 0.276(1)$ for $\beta_g = 0.5$ and $\beta_g = 1$, respectively.

where $F(x)$ is a universal scaling function. As in our previous work [15], we will use Eq. (25) to perform a direct check of universality, because no model-dependent normalizations enter: If two models belong to the same universality class, the data for both of them should collapse onto the same curve as L increases. The only difficulty in the approach is that one should be careful in identifying corresponding operators in the two models.

To identify the correct operators, one may reason as follows. In the AH lattice model the basic quantity that we consider is the local operator (13). To identify the corresponding operator in the Heisenberg model, we use the explicit relation between the CP^1 and the O(3) vector model. Under the mapping, the parameter U and ξ correspond to the usual O(3) vector Binder parameter and correlation length (i.e., computed from correlations of the fundamental spin variable $\boldsymbol{s}_x$). The mapping of the large-β_g limit of the AH lattice model into the O(4) vector model is instead more complex and is discussed in detail in Appendix B. The correspondence is not trivial and U is identified with a combination of suitably defined O(4) tensor Binder parameters.

In Fig. 2 we plot R_ξ versus β, for several values of L. The data for different values of the size L show crossing points,

which provide estimates of the critical point: $\beta_c = 0.4145(5)$ and $\beta_c = 0.276(1)$ for $\beta_g = 0.5$ and $\beta_g = 1$, respectively. Data are consistent with a continuous transition.

We now argue that the transitions are consistent with the expected asymptotic Heisenberg behavior. The best evidence is provided by the plots of U versus R_ξ; see Fig. 3. In all panels we report the data and the corresponding O(3) curve. If our simple scenario is correct, the data for all values of β_g must approach the O(3) curve with increasing L. For $\beta_g = 0$ we observe very good agreement, as already discussed in Ref. [15]. For $\beta_g = 0.5$ convergence is slower, indicating that scaling corrections increase with increasing β_g. For $R_\xi \lesssim 0.25$ we observe a good collapse of the data, while in the opposite case, we observe a clear upward trend, consistent with an asymptotic O(3) behavior. For $\beta_g = 1$, for small values of L we observe significant differences between data and O(3) curve. These discrepancies decrease as L increases and can therefore be interpreted as scaling corrections. For $R_\xi \lesssim 0.25$, the results for $L = 64$ fall on top of the O(3) scaling curve, as predicted. For larger values of R_ξ, crossover effects are stronger, but the trend of the data is the expected one.

To be more quantitative, let us note that, for large values of L, the Binder parameter U should behave as [20]

$$U(\beta, \beta_g, L) = F(R_\xi) + a(\beta_g)\, G(R_\xi)\, L^{-\omega} + \cdots , \qquad (26)$$

where $F(R_\xi)$ is the O(3) scaling function, $G(R_\xi)$ is a universal function, and $a(\beta_g)$ is a constant that encodes the β_g-dependent size of the leading scaling corrections decaying as $L^{-\omega}$. We have verified that our data for $\beta_g = 0.5$ and 1 are consistent with Eq. (26), if we take $\omega = 0.78$ (the leading correction-to-scaling exponent in Heisenberg systems [20,42–44]) and $a(1)/a(0.5) \approx 5$. This can be checked from Fig. 4, where we report

$$\Delta(\beta, \beta_g, L) = \frac{1}{a(\beta_g)} L^{\omega} [U(\beta, \beta_g, L) - F(R_\xi)], \qquad (27)$$

where $F(R_\xi)$ has been determined in the O(3) vector model, $\omega = 0.78$, $a(1) = 5$, and $a(0.5) = 1$. All data reported in the figure are consistent with a single scaling curve that would be identified with the function $G(R_\xi)$ in Eq. (26). The existence of similar crossover effects for $\beta_g = 0.5$ and 1 is another demonstration of universality.

It is interesting to note that the behavior of the data for small L at $\beta_g = 1$ can be interpreted as due to the presence of O(4) fixed point that controls the critical behavior for $\beta_g \to \infty$. In the lower panel of Fig. 3, we also plot the O(4) scaling curve. The data for $\beta_g = 1$ apparently follow the O(4) curve for small lattice sizes and then move toward the O(3) curve with increasing L. In particular, note the nonmotonic behavior of the data for small lattice sizes and $R_\xi \approx 0.1$, similar to the one that characterizes the O(4) curve. Such a behavior disappears with increasing L (see the inset in the lower panel of Fig. 3).

On the basis of the above numerical results we argue that the finite-temperature transition is continuous for any finite $\beta_g \geqslant 0$ and belongs to the Heisenberg universality class. However, for relatively large values of β_g, say $\beta_g \gtrsim 1$, notable crossover effects emerge. They are apparently related to the presence of the O(4) fixed point, which is the relevant one for $\beta_g \to \infty$. For large values of β_g, such effects may hide the asymptotic Heisenberg behavior. For intermediate sizes, data are expected to show an effective O(4) critical behavior, converging to the Heisenberg behavior only for very large lattices.

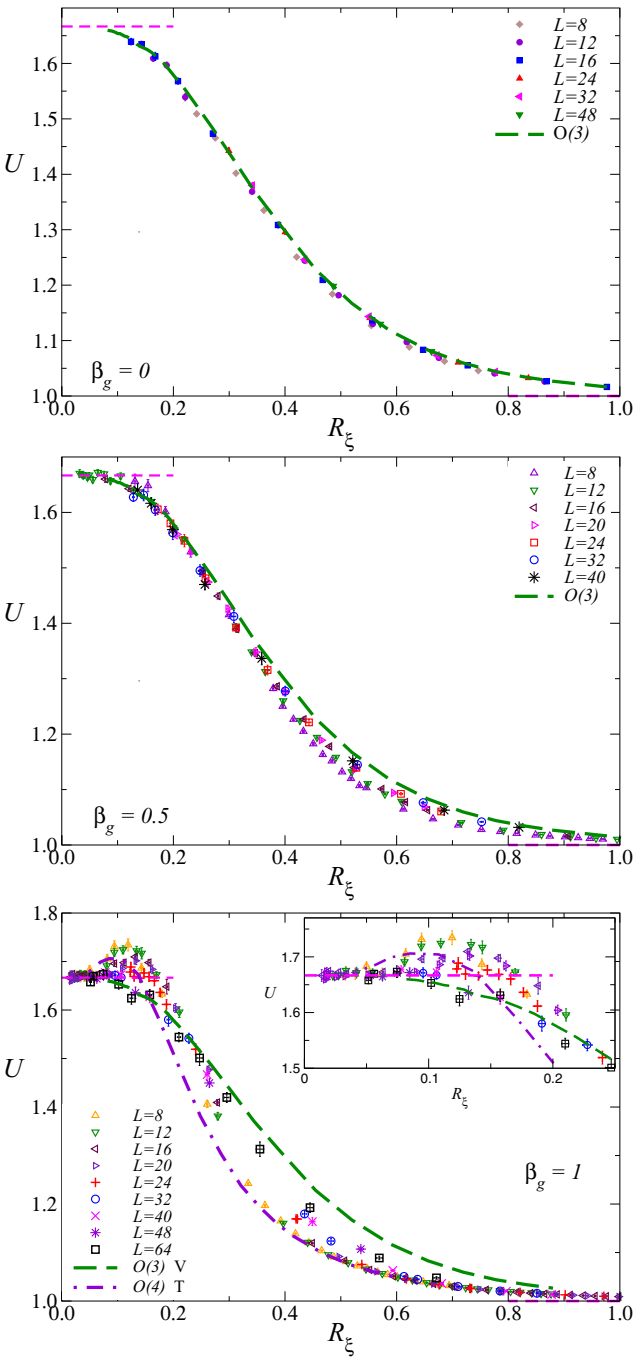

FIG. 3. The Binder parameter U versus R_ξ in the $N = 2$ AH lattice model, for $\beta_g = 0$ (top, data from Ref. [15]), $\beta_g = 0.5$ (middle), and $\beta_g = 1$ (bottom). In all panels the dashed line is the Heisenberg curve, as obtained from MC simulations of the O(3) vector model. The dot-dashed line in the lower panel is the limiting curve for $\beta_g \to \infty$ (see Appendix B). The inset enlarges the region $R_\xi < 0.25$, showing that the nonmotonic behavior that characterizes the small-size data [similar to the one of the O(4) curve] for $R_\xi \approx 0.1$ disappears with increasing L. The horizontal dashed line shows the asymptotic value $U(R_\xi \to 0) = 5/3$.

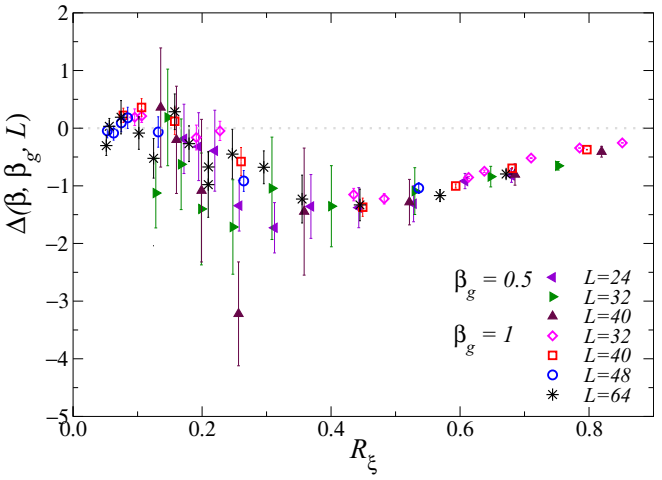

FIG. 4. The quantity $\Delta(\beta, \beta_g, L)$ defined in Eq. (27) versus R_ξ. We report data for $\beta_g = 1$ and 0.5 and several values of L.

C. First-order transitions for $N = 4$

We now discuss the behavior of the $N = 4$ AH lattice model, providing evidence that the transitions along the line separating the two phases are of first order for any finite β_g. Only when β_g is strictly infinity is the transition continuous: it belongs to the O(8) vector universality class.

As shown in Ref. [15], the transition is of first order for $\beta_g = 0$. To show that the nature of the transition is unchanged for $\beta_g > 0$, we first consider the specific heat and the Binder parameter U. Both of them are expected to increase as the volume at a first-order transition. Indeed, according to the standard phenomenological theory [45], for a lattice of size L there exists a value $\beta_{\max,C}(L)$ of β where C takes its maximum value $C_{\max}(L)$, which asymptotically increases as

$$C_{\max}(L) = V\left[\tfrac{1}{4}\Delta_h^2 + O(1/V)\right], \tag{28}$$

$$\beta_{\max,C}(L) - \beta_c \approx c\, V^{-1}; \tag{29}$$

here $V = L^d$ and Δ_h is the latent heat [defined as $\Delta_h = E(\beta \to \beta_c^+) - E(\beta \to \beta_c^-)$]. Analogously, the behavior of the Binder parameter $U(\beta, L)$ is expected to show a maximum $U_{\max}(L)$ at fixed L (for sufficiently large L) at $\beta = \beta_{\max,U}(L) < \beta_c$ with [15,33,46]

$$U_{\max} \sim a\, V + O(1), \tag{30}$$

$$\beta_{\max,U}(L) - \beta_c \approx b\, V^{-1}. \tag{31}$$

The previous relations are valid in the asymptotic limit and, for weak transitions, require data on large lattices. As we discussed in Ref. [15], one can identify first-order transitions on significantly smaller lattices from the analysis of the behavior of the Binder parameter U. In the presence of a first-order transition, one observes large violations of the scaling relation (25) for values of L that are significantly smaller than those at which relations (28) and (31) hold. We will follow this approach here, considering again two values of β_g, 0.5 and 1.

In Fig. 5 we report numerical estimates of U at $\beta_g = 0$ (taken from Ref. [15]), $\beta_g = 0.5$, and $\beta_g = 1$. Clearly,

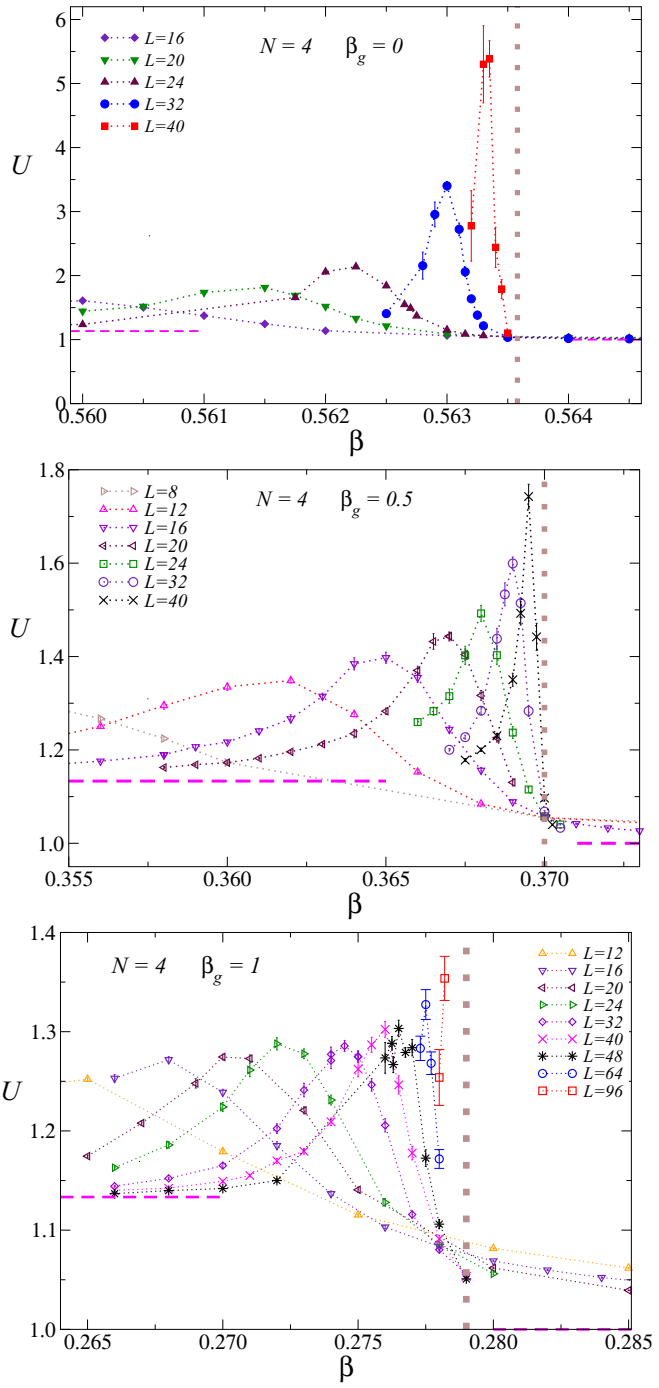

FIG. 5. Plot of the Binder parameter U versus β, for $\beta_g = 0$ (top, from Ref. [15]), $\beta_g = 1/2$ (middle), and $\beta_g = 1$ (bottom), for $N = 4$. The vertical lines correspond to the estimates of the transition points. The horizontal dashed lines show the values $U(\beta \to 0) = 17/15$ and $U(\beta \to \infty) = 1$.

the maximum $U_{\max}$ increases with increasing L, as expected for a first-order transition. However, with increasing β_g, the rate of increase becomes smaller, indicating that the transition becomes weaker. The specific heat behaves analogously.

To obtain a better evidence that the finite-size behavior is not compatible with a continuous transition, we plot U versus

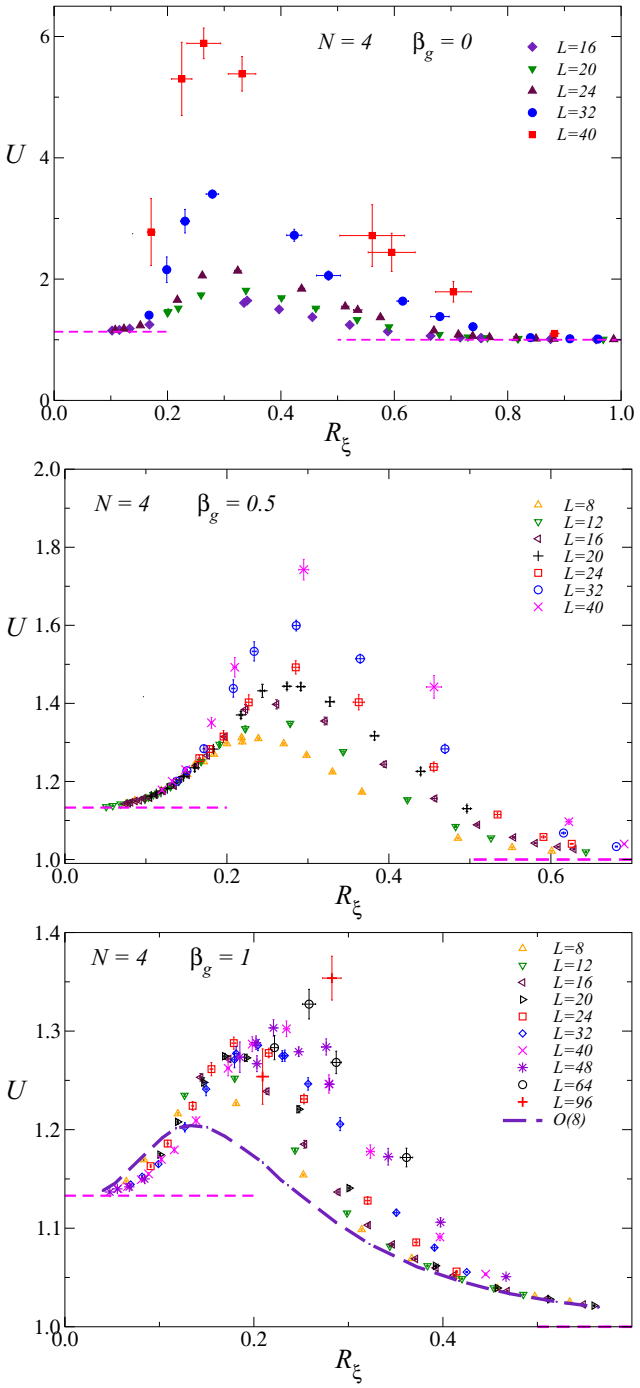

FIG. 6. The Binder parameter U versus R_ξ versus β, for $\beta_g = 0$ (top, from Ref. [15]), $\beta_g = 1/2$ (middle), and $\beta_g = 1$ (bottom) for $N = 4$. The dashed line in the lower panel is the O(8) limiting scaling curve; see Appendix B. The horizontal dashed lines show the asymptotic values $U(R_\xi \to 0) = 17/15$ and $U(R_\xi \to \infty) = 1$.

R_ξ; see Fig. 6. Data do not show any scaling behavior, as expected at a first-order transition.

Note that for $\beta_g = 1$ the small size data show an apparent scaling behavior for small values of R_ξ and small L, which may lead to erroneous conclusions when limiting the FSS analysis to small lattices (as in Ref. [6]). To clarify the origin of the transient effects, and understand whether they can be interpreted as due to the O(8) fixed point that controls the

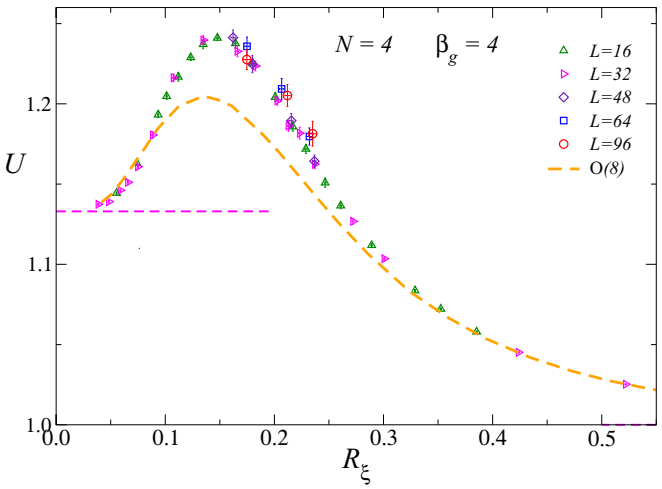

FIG. 7. The Binder parameter U versus R_ξ for $\beta_g = 4$ and $N = 4$. The dashed line is the O(8) limiting scaling curve; see Appendix B. The horizontal dashed line indicates the asymptotic value $U(R_\xi \to 0) = 17/15$.

behavior for $\beta_g = \infty$, we have performed MC simulations for $\beta_g = 4$. This value is so large that, for our range of values of L, we do not expect to observe effects related to the first-order nature of the transition and therefore all data should be in the crossover region. The analysis of U as a function of β allows us to estimate $\beta_c = 0.2484(2)$, which is close to the O(8) value, $\beta_c \approx 0.2408$. At the transition, gauge fields are significantly ordered and indeed, the average value of the product of the gauge fields along an elementary plaquette (a Wilson loop of size 1) is 0.95780(5) (for comparison, such a product is equal to 0.8235(5) at the transition for $\beta_g = 1$). In Fig. 7 we report U versus R_ξ and compare it with the O(8) curve. The numerical data with $16 \leqslant L \leqslant 48$ apparently fall onto a single scaling curve, while the data corresponding to $L = 64$ and 96 begin to show the drift that characterizes the results at $\beta_g \leqslant 1$ and which is related to the asymptotic first-order nature of the transition. The apparent scaling curve for small values of L is different from the O(8) one, indicating that for $\beta_g = 4$ we are observing a sizable contribution due the relevant operator that destabilizes the O(8) fixed point for finite β_g. We can also infer from the substantial stability of the results for $L \leqslant 48$ that it has a very small (positive) scaling dimensions y. Indeed, close to the O(8) fixed point, we expect

$$U(\beta, \beta_g) = F(R_\xi, b(\beta_g, \beta) L^y), \tag{32}$$

where $b(\beta_g, \beta)$ is a nonuniversal amplitude, which vanishes for $\beta_g \to \infty$. For each β_g the crossover region is the one in which $b(\beta_g, \beta_c) L^y \ll 1$. If this condition holds, U can be written as

$$U(\beta, \beta_g) = F(R_\xi, 0) + b(\beta_g, \beta) L^y G(R_\xi), \tag{33}$$

where the first term is the O(8) scaling function. This equation would imply that the deviations from the O(8) behavior scale, at least for β_g very large, as L^y. Our results therefore imply that y should be small enough, so that L^y does not change significantly as L varies from 16 to 48.

In conclusion, the numerical results favor a phase diagram based on a first-order transition line for $\beta_g > 0$, starting from

the first-order transition of the CP^3 models, corresponding to $\beta_g = 0$. With increasing β_g the first-order transition becomes weaker. We observe substantial crossover phenomena for $\beta_g \gtrsim 1$. They may be explained in terms of the O(8) fixed point controlling the behavior for $\beta_g \to \infty$, perturbed by a relevant operator with a relatively small scaling dimension.

D. Vector and gauge observables

In the previous sections we discussed the behavior of quantities defined in terms of the gauge-invariant order parameter $Q_{\boldsymbol{x}}^{ab}$. Here we discuss instead the vector correlation function (20) and the gauge observables (21) and (22). We focus on $N = 4$.

Let us first discuss their behavior in the two different phases. In the high-temperature phase $\beta < \beta_c$, we find that the correlation function can be approximated as ($x > 0$)

$$G_V(x, L) = Ae^{-x/\xi_z}, \tag{34}$$

as soon as x is 2 or 3. Moreover, for small β, ξ_z is very little dependent on β_g. For instance, for $\beta = 0.1$, the strong-coupling behavior $G_V(x, L) \sim (N\beta)^x$ holds quite precisely for all values of β_g. Wilson loops behave in a very similar fashion. We find $W(m, L) \approx B \exp(-4m/\xi_w)$ with $\xi_w \approx \xi_z$ as long as $m \gtrsim 2$. Clearly, in the high-temperature phase a single gauge mode controls the behavior of all observables that involve gauge degrees of freedom.

The behavior in the low-temperature phase is analogous. The correlation function $G_V(x, L)$ behaves as in Eq. (34); see the upper panel of Fig. 8 for results at $\beta = 0.8$. Moreover, Polyakov and Wilson loops satisfy

$$P(L) = Ae^{-L/\xi_z}, \quad W(m) = Be^{-4m/\xi_z}, \tag{35}$$

with the same correlation length and $A, B \approx 1$. Figure 8 also shows that $G_V(x, L)$ has a very precise exponential decay even when $\xi_z \gtrsim L$. Clearly, it couples to a single isolated mode and hence there are no corrections to the leading exponential behavior. In this phase the correlation length increases with β_g (see the lower panel of Fig. 8): in agreement with perturbation theory, it scales linearly with β_g in the limit $\beta_g \to \infty$. Note the ξ_z is also expected to diverge in the limit $\beta \to \infty$ at fixed β_g. Indeed, for $\beta \to \infty$, the relevant configurations are those that minimize the Hamiltonian term that depends on the fields z. If we perform a local minimization on each link, we find the constraint

$$z_{\boldsymbol{x}+\hat{\mu}} = \bar{\lambda}_{\boldsymbol{x},\mu} z_{\boldsymbol{x}}. \tag{36}$$

This constraint can be satisfied simultaneously on the four links belonging to a plaquette only if the product of the gauge fields along the plaquette is 1. Analogously, the constraint is satisfied on the links that belong to a loop that wraps around the lattice only if the Polyakov operator is 1. It follows that gauge configurations are trivial—$\lambda_{\boldsymbol{x},\mu}$ is 1 on all links modulo gauge transformations—and ξ_z is infinite in this limit.

These results for the gauge observables indicate that gauge and vector observables are noncritical in both phases and that their behavior is analogous for small and large values of β. Only the limit $\beta_g \to \infty$ distinguishes the two sectors. If $\beta_{c,\infty}$ is the transition point for $\beta_g \to \infty$ [therefore in the O($2N$) theory], for $\beta_g \to \infty$, the correlation length ξ_z is finite for $\beta < \beta_{c,\infty}$ and infinite in the opposite case. This guarantees that vector correlations are critical in the O($2N$) theory with a finite low-temperature magnetization. But this occurs only for β_g strictly equal to infinity. For finite β_g, only Q correlations display criticality.

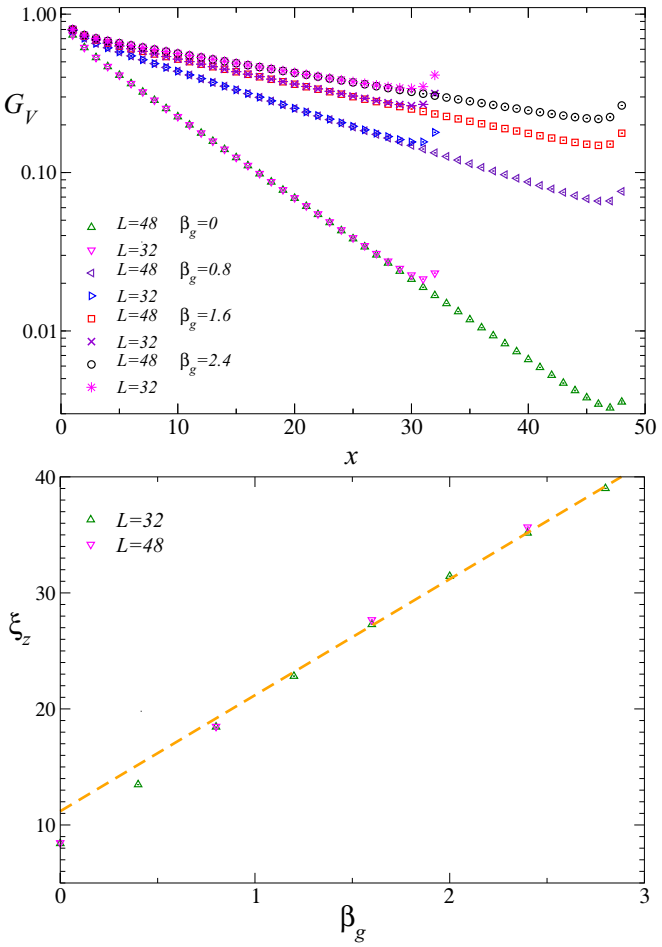

FIG. 8. Top: Vector correlation function $G_V(x, L)$ versus x for $\beta = 0.8$ and several values fo β_g. Bottom: Vector correlation length ξ_z as a function of β_g for $\beta = 0.8$. The line shows that ξ_z scales as β_g for large β_g (the parameters have been determined by performing a linear fit of the data with $\beta_g \geqslant 1.6$). For $x = L$, $G_V(L, L)$ corresponds to the average of the Polyakov loop.

Finally, let us discuss the behavior of vector and gauge quantities along the transition line. For $N = 4$, as we are dealing with first-order transitions, we expect $G_V(x, L)$ to depend on the phase one considers. In the CP^3 model ($\beta_g = 0$) the transition is strong and therefore the high-temperature (HT) and low-temperature (LT) correlation functions can be easily computed by fixing β in the coexistence region and starting the simulation from a random or an ordered configuration. We find that in both cases the correlation function decays very rapidly and estimate $\xi_z \approx 1.9$ and $\xi_z \approx 1.7$ in the LT and HT phase, respectively. Clearly, vector modes are not critical. Similar results hold for the CP^1 and CP^2 models. In the first case, we obtain $\xi_z \approx 2.2$. For $N = 3$ the transition is so weak that we cannot identify the two phases and we are only able to compute an effective correlation function, which is a linear combination of those appropriate for the two phases.

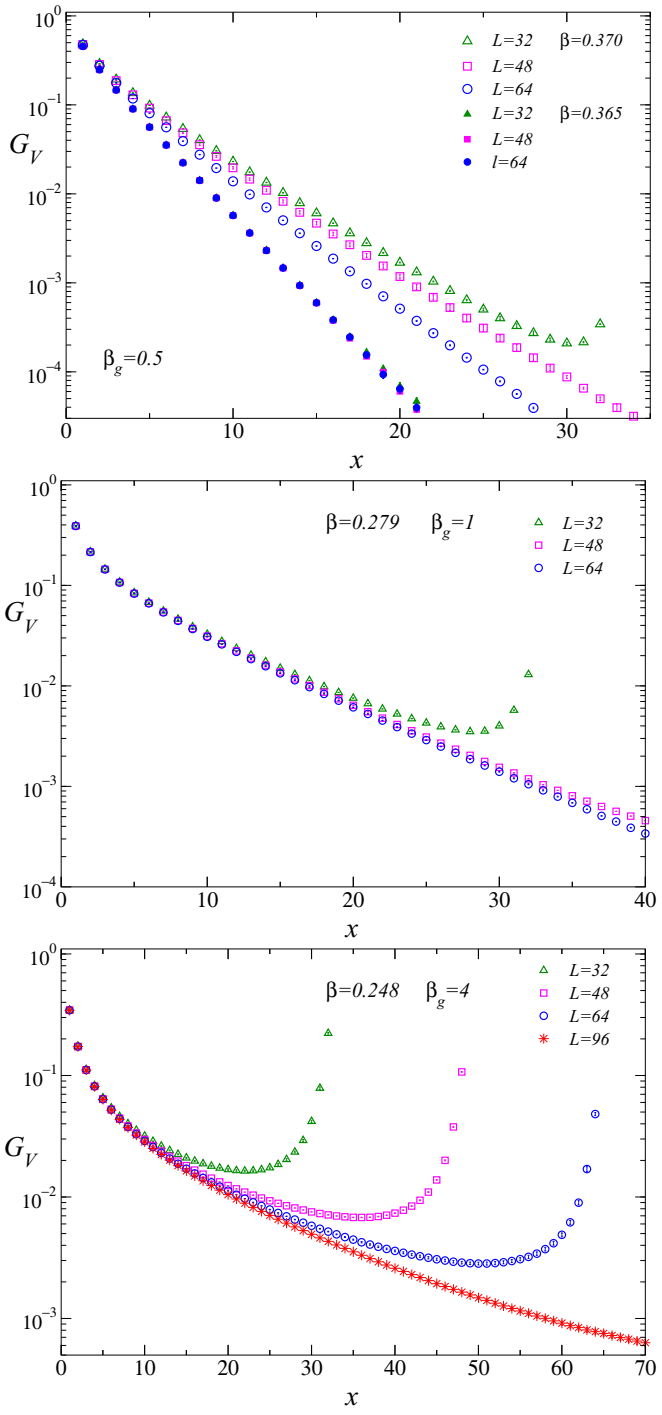

FIG. 9. The vector correlation function $G_V(x, L)$ in the critical region for $\beta_g = 0.5$ (top), 1 (middle), and 4 (bottom). For $\beta_g = 0.5$ we report the estimate for $\beta = 0.365$ (high-temperature phase) and for $\beta = 0.370$ (low-temperature phase). For $\beta_g = 1$ and 4, we report an effective estimate of the correlation function in the coexistence region (see text for a discussion), computed at $\beta = 0.279$ for $\beta_g = 1$, and at $\beta = 0.248$ for $\beta_g = 4$.

This quantity still allows us to compute the largest of the two correlation lengths, i.e., ξ_z in the LT phase, obtaining $\xi_z \approx 2.2$. Results for finite β_g are reported in Fig. 9. The first distinctive feature is that, for the cases we consider, the correlation function does not behave as a single exponential, although an exponential behavior sets in when $x \gg \xi_z$. Clearly, at the critical point several modes are playing an important role and an exponential behavior is only observed when ξ_z is significantly less than L. Second, the correlation length ξ_z increases with increasing β_g along the transition line. For $\beta_g = 0.5$ we obtain $\xi_z \approx 3.8$, 3.6, 3.1 for $L = 32$, 48, and 64 in the LT phase (runs at $\beta = 0.370$ with ordered start). In the HT phase (runs at $\beta = 0.365$ starting from a random configuration) we obtain $\xi_z \approx 2.2$ with a small L dependence. Although ξ_z is small, it is larger than the value it takes in the CP^3 model, i.e. the AH model with $\beta_g = 0$. For $\beta_g = 1$, we are not able to distinguish the two phases and, therefore, we only compute the LT estimate of ξ_z. Results for $L = 32, 48, 64$ essentially agree and give $\xi_z \approx 6.9$. This estimate is confirmed by the analysis of the Polyakov loop. A fit to Eq. (35) gives $\xi_z = 6.9(1)$, in very good agreement with the results obtained from $G_V(x)$. For $\beta_g = 4$, even for $L = 96$ we are not yet in the regime in which one can reliably identify a range of distances in which the correlation function decays exponentially. If we fit the correlation function to Eq. (34) in the range $L/3 \leqslant 2L/3$, we obtain $\xi_z = 17.1(1)$ and 17.6(1) for $L = 64$ and 96, respectively. The analysis of the Polyakov loop gives a somewhat larger value $\xi_z = 20.9(3)$. Whatever the exact asymptotic result is, data confirm that, for $\beta_g = 4$, we are deep in the crossover region, where vector and gauge excitations compete with gauge-invariant excitations associated with Q_x (for comparison note that $\xi = 20.3(3)$ for $L = 96$). These results provide us a physical explanation of the crossover effects we observe. The asymptotic first-order behavior is observed only when the correlation length $\xi(L)$ at the transition point is significantly larger than ξ_z. When $\xi(L) \sim \xi_z$ we observe an apparent scaling behavior in which both the (gauge-field independent) degrees of freedom associated with Q and the (gauge-field dependent) ones, that are encoded in the gauge observables and in the vector correlations, are both relevant.

IV. CONCLUSIONS

We have studied the phase diagram and critical behavior of muticomponent AH lattice models, in which an N-component complex field z_x is coupled to quantum electrodynamics. We consider the compact Wilson formulation of Abelian lattice gauge theories in which the fundamental gauge fields are complex numbers of unit modulus; see Eq. (3). For the scalar fields, we consider the unit-length limit and fix $|z_x|^2 = 1$. Finally, we fix $q = 1$ for the charge of the matter fields. We focus on systems with a small number of components, considering $N = 2$ and $N = 4$.

We investigate the phase diagram of the model as a function of the couplings β and β_g. The phase diagram is characterized by two phases: a low-temperature phase (large β) in which the order parameter Q^{ab} condenses, and a high-temperature disordered phase (small β). The gauge coupling does not play any particular role in the two phases: gauge observables and vector observables do not show long-range correlations for any finite β and β_g. The two phases are separated by a transition line that connects the CP^{N-1} transition point ($\beta_g = 0$) with the O($2N$) transition point ($\beta_g = \infty$). Concerning the nature of the transition line, our numerical

data are consistent with a simple scenario, in which the nature of the transition line is independent of β_g. Therefore, we predict Heisenberg critical behavior along the whole line for $N = 2$, and first-order transitions for $N = 4$. Note that, for $\beta_g \to \infty$ the model becomes equivalent to the O($2N$) vector model, and therefore one expects strong crossover effects controlled by the O($2N$) fixed point. These crossover effects are related to the presence of a second length scale ξ_z associated with the vector correlations, which is finite for any β_g and diverges in the limit $\beta_g \to \infty$ in the whole low-temperature phase.

The scenario supported by our numerical data is fully consistent with the LGW approach that assumes a gauge-invariant order parameter. On the other hand, at least for $N = 2$, it disagrees with the ε-expansion predictions obtained using the standard continuum AH model: for $N = 2$ this approach does not predict a continuous transition. Numerical results allow us to understand why the LGW approach is more appropriate than the continuum AH model for these values of N. At the transition (for both $N = 2$ and $N = 4$) only correlations of the gauge-invariant operator Q^{ab} display long-range order. Gauge modes represent a background that gives only rise to crossover effects and indeed, the asymptotic behavior sets in only when the correlation length of the gauge fluctuations is negligible compared to that of the Q correlations. It is important to note that a LGW approach based on a gauge-invariant order parameter has also been applied to the study of phase transitions in the presence of non-Abelian gauge symmetries, and, in particular, to the study of the finite-temperature transition of hadronic matter as described by the theory of strong interactions, quantum chromodynamics [47–49]. Our results for the AH lattice model lend support to the correctness of the approach and of the predictions obtained.

We expect that AH lattice models with higher (but not too large) values of N have a phase diagram similar to the one obtained for $N = 4$, with a first-order transition line separating the ordered and disordered phases. The phase diagram may change for large values of N. In this regime, the system may undergo continuous transitions controlled by the stable fixed point of the continuum AH model. This issue requires additional investigations.

It is important to stress that we have considered here a compact version of electrodynamics. Other models of interest in condensed-matter physics consider complex fields (spinons) coupled to noncompact electrodynamics [5,50,51]. Such a model may have a different critical behavior due the suppression of monopoles [52–55]. Numerical studies have identified the transition, but at present there is no consensus on its order. The same is true for loop models which supposedly belong to the same universality class (if it exists); see, e.g., Refs. [4,16,17,56,57]. Clearly, additional work is needed to settle the question.

APPENDIX A: TENSOR SCALING FUNCTIONS IN THE n-VECTOR MODEL

In this Appendix we compute the scaling functions of tensor observables in the three-dimensional n-vector model, as they are relevant for the discussion of the large-β_g limit of CP^{N-1} models. We consider a cubic lattice and define an n-dimensional real spin vector $s_{\boldsymbol{x}}^{\alpha}$ on each lattice site. The Hamiltonian is

$$\mathcal{H} = -\beta n \sum_{\langle \boldsymbol{x}\boldsymbol{y}\rangle} \boldsymbol{s}_{\boldsymbol{x}} \cdot \boldsymbol{s}_{\boldsymbol{y}}, \tag{A1}$$

where the sum extends over all lattice nearest-neighbor pairs $\langle \boldsymbol{x}\boldsymbol{y}\rangle$. We define the tensor (matrix) field

$$T_{\boldsymbol{x}}^{\alpha\beta} = s_{\boldsymbol{x}}^{\alpha} s_{\boldsymbol{x}}^{\beta} - \frac{1}{n}\delta^{\alpha\beta}, \tag{A2}$$

the vector and tensor correlation functions

$$\begin{aligned} G_V(\boldsymbol{x}) &= \langle \boldsymbol{s}_{\boldsymbol{0}} \cdot \boldsymbol{s}_{\boldsymbol{x}} \rangle, \\ G_T(\boldsymbol{x}) &= \sum_{\alpha\beta} \left\langle T_{\boldsymbol{0}}^{\alpha\beta} T_{\boldsymbol{x}}^{\alpha\beta} \right\rangle = \langle \mathrm{Tr}\,(T_{\boldsymbol{0}} T_{\boldsymbol{x}}) \rangle, \end{aligned} \tag{A3}$$

where "Tr" is the trace over the $O(n)$ indices, and the corresponding correlation lengths ξ_V and ξ_T, defined as in Eq. (17). We also consider renormalization-group invariant ratios (collectively named Binder parameters) defined in terms of

$$\Theta^{\alpha\beta} = \sum_{\boldsymbol{x}} T_{\boldsymbol{x}}^{\alpha\beta}. \tag{A4}$$

We define

$$U_{3T} = \frac{\langle \mathrm{Tr}\,\Theta^3 \rangle}{\langle \mathrm{Tr}\,\Theta^2 \rangle^{3/2}}, \tag{A5}$$

$$U_{4T,a} = \frac{\langle [\mathrm{Tr}\,\Theta^2]^2 \rangle}{\langle \mathrm{Tr}\,\Theta^2 \rangle^2}, \quad U_{4T,b} = \frac{\langle \mathrm{Tr}\,\Theta^4 \rangle}{\langle \mathrm{Tr}\,\Theta^2 \rangle^2}. \tag{A6}$$

These quantities are not independent for $n = 2$ and 3. The relation $U_{4T,b} = U_{4T,a}/2$ holds for $n = 2, 3$, while $U_3 = 0$ for $n = 2$.

We can easily predict the value the Binder parameters take in the high-temperature phase. The cubic parameter U_{3T} vanishes, while

$$U_{4T,a} = \frac{n^2 + n + 2}{(n+2)(n-1)}, \quad U_{4T,b} = \frac{2n^2 + 3n - 6}{n(n+2)(n-1)}. \tag{A7}$$

In the low-temperature phase we obtain instead

$$U_{3T} = \frac{n-2}{\sqrt{n(n-1)}}, \tag{A8}$$

$$U_{4T,a} = 1, \quad U_{4T,b} = \frac{n^2 - 3n + 3}{n(n-1)}. \tag{A9}$$

We have computed the scaling functions for the Binder parameters and ξ_T/L for $n = 3, 4, 5, 8$ on cubic lattices of size L, with L in the interval $16 \leqslant L \leqslant 32$. We use periodic boundary conditions. In Figs. 10 and 11 we report the scaling functions as a function of X defined in Eq. (23) . We have used the following values for $\overline{\beta}_c = n\beta_c$ and ν: $\overline{\beta}_c = 0.69302(3)$ [40,58] and $\nu = 0.7112(5)$ [43] for $n = 3$; $\overline{\beta}_c = 0.93586(1)$ [40,41] and $\nu = 0.749(2)$ [59] for $n = 4$; $\overline{\beta}_c = 1.18138(3)$ and $\nu = 0.779(3)$ [60] for $n = 5$; $\overline{\beta}_c = 1.92677(2)$ and $\nu = 0.85(2)$ [18] for $n = 8$. Note that, on the scale of the figure, differences on the value of ν of 1% cannot be distinguished.

In spite of the fact that lattices are relatively small, we observe a very good scaling. We have also determined the value of the different quantities at the critical point;

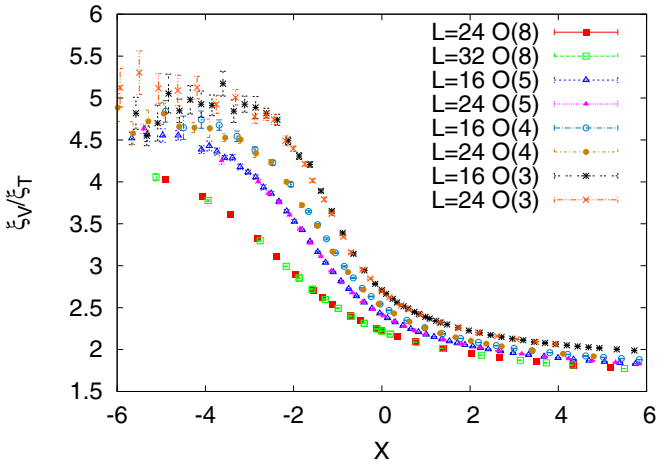

FIG. 10. Plot of ξ_V/ξ_T as a function of $X = (\beta - \beta_c)L^{1/\nu}$ for $n = 3$, 4, 5, and 8.

see Table I. The results have been obtained by extrapolating the finite-L data assuming that scaling corrections behave as $L^{-\omega}$. The quoted error includes the statistical error, the interpolation error of the data, the error on β_c and ν, and the extrapolation error. The latter has been conservatively estimated as the difference between the extrapolated value and the value that the observable takes on the largest lattice.

TABLE I. Estimates of several renormalization-group invariant quantities at the critical point $X = 0$.

	$n = 3$	$n = 4$	$n = 5$	$n = 8$
$U^*_{4T,a}$	1.458(12)	1.287(7)	1.218(2)	1.117(2)
$U^*_{4T,b}$	0.729(6)	0.684(2)	0.677(3)	0.681(2)
U^*_{3T}	0.334(10)	0.462(7)	0.529(3)	0.636(2)
$(\xi_T/L)^*$	0.213(5)	0.221(4)	0.222(1)	0.236(1)
$(\xi_V/\xi_T)^*$	2.68(3)	2.50(2)	2.41(1)	2.21(1)

In Fig. 12 we report the same invariant ratios as a function of ξ_T/L. Some numerical values (extrapolations and errors have been computed as before) are reported in Table II.

APPENDIX B: FINITE-SIZE SCALING BEHAVIOR FOR $\beta_g \to \infty$

In this Appendix we discuss the limit $\beta_g \to \infty$ of the model. In this limit, the gauge part of the Hamiltonian becomes trivial and we obtain

$$\lambda_{\boldsymbol{x},\mu}\, \lambda_{\boldsymbol{x}+\hat{\mu},\nu}\, \bar{\lambda}_{\boldsymbol{x}+\hat{\nu},\mu}\, \bar{\lambda}_{\boldsymbol{x},\nu} = 1 \qquad \text{(B1)}$$

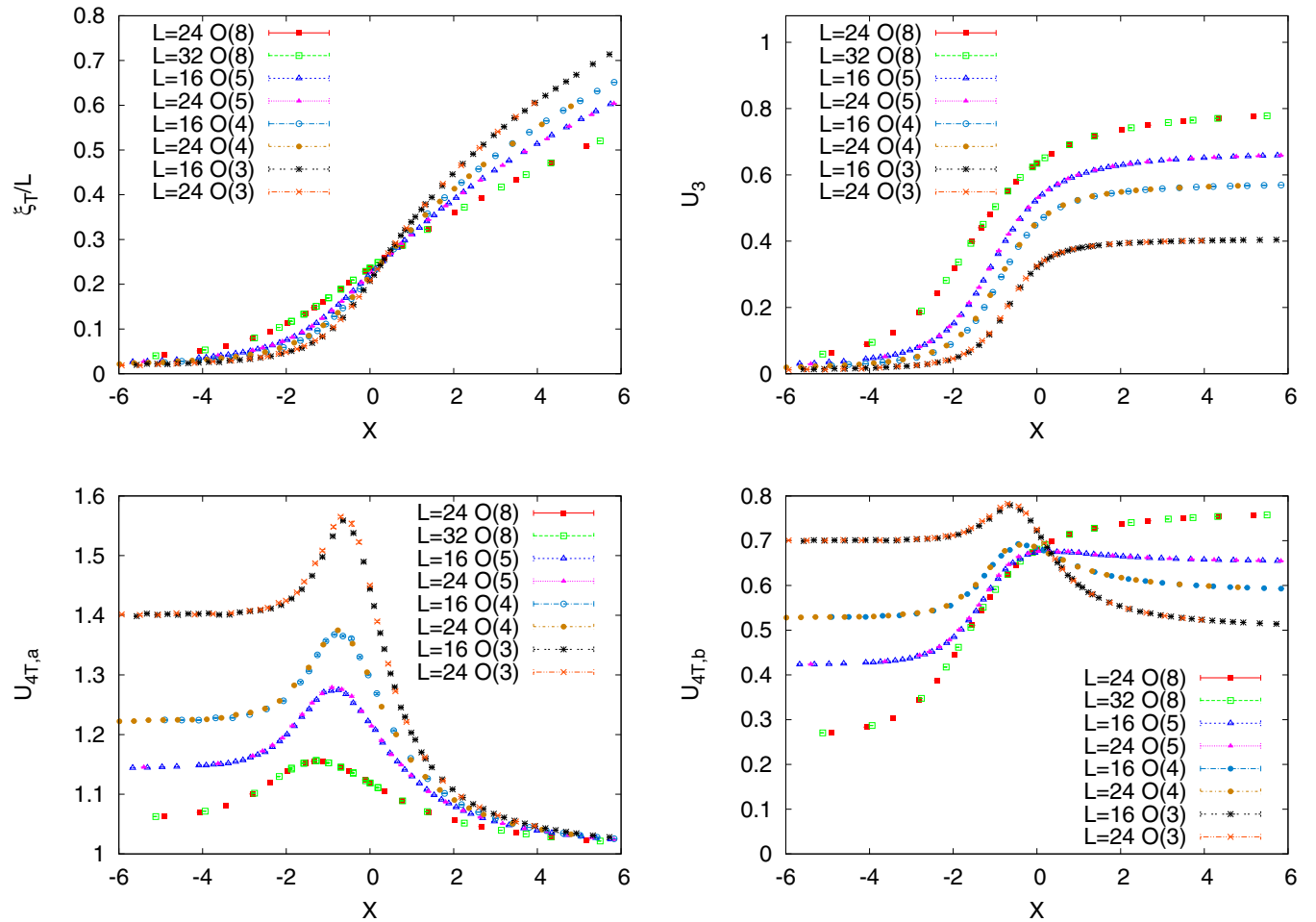

FIG. 11. Plot of ξ_T/L (top left), U_{3T} (top right), $U_{4T,a}$ (bottom left), and $U_{4T,b}$ (top right) as a function of $X = (\beta - \beta_c)L^{1/\nu}$ for $n = 3$, 4, 5, and 8.

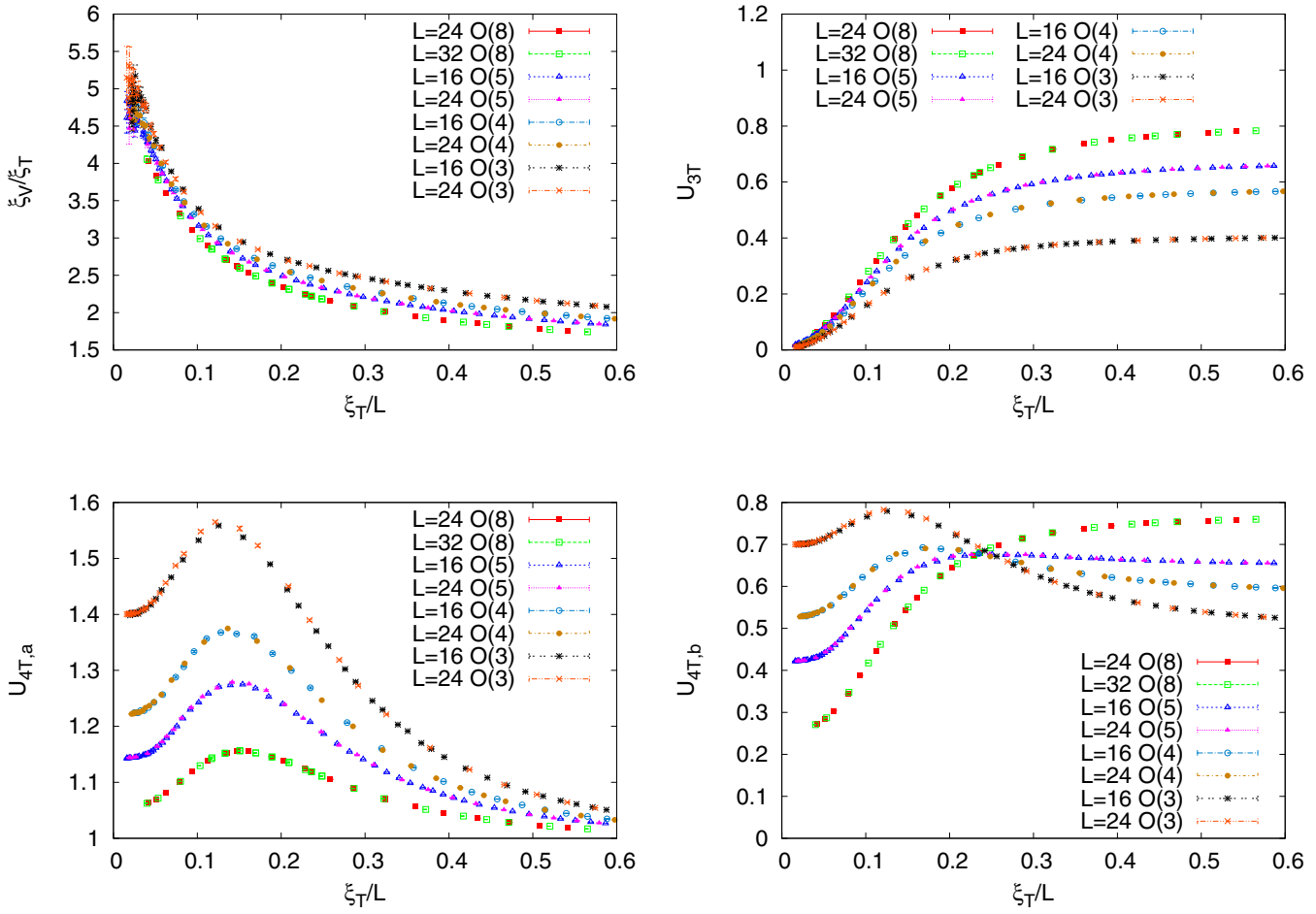

FIG. 12. Plot of ξ_V/ξ_T (top left), U_{3T} (top right), $U_{4T,a}$ (bottom left), and $U_{4T,b}$ (top right) as a function of ξ_T/L for $n = 3$, 4, 5, and 8.

on every lattice plaquette. We consider a finite lattice with periodic boundary conditions and further assume that the Polyakov loops order in the same limit. If this occurs (we discuss this issue in Sec. III D), we can set $\lambda_{x,\mu} = 1$ on each lattice link. Therefore, for $\beta_g \to \infty$, the Hamiltonian becomes simply

$$H = -\beta N \sum_{x,\mu} (\bar{z}_x \cdot z_{x+\hat{\mu}} + \text{c.c.}). \tag{B2}$$

We now define a $2N$-dimensional unit real vector s_x by setting

$$z_x^a = s_x^a + i s_x^{a+N}, \tag{B3}$$

$a = 1, \ldots, N$. In terms of this new field the Hamiltonian becomes that of the n vector model [see Eq. (A1)], with $n = 2N$. We have therefore an enlargement of the global symmetry: the model is now invariant under O($2N$) transformations.

Since the model becomes O($2N$) invariant, it is useful to rewrite CP^{N-1} observables in terms of explicitly O($2N$) invariant quantities that can be determined directly in the O($2N$) theory. The basic CP^{N-1} variable Q_x^{ab} can be rewritten in terms of the tensor operator $T_x^{\alpha\beta}$ of the O($2N$) theory. The relation is not trivial,

$$Q_x^{ab} = T_x^{ab} + T_x^{a+N,b+N} + i T_x^{a,b+N} - i T_x^{a+N,b}, \tag{B4}$$

which implies that Q-correlations are not trivially related to T correlations in the vector model. Using relation (B4), we can express the CP^{N-1} correlation function $G(x)$ in terms of the O($2N$) tensor correlation function $G_T(x)$. Using the O($2N$) invariance of the model we obtain

$$G(x) = \frac{2(N-1)}{2N-1} G_T(x), \tag{B5}$$

which implies that the CP^{N-1} correlation length can be identified with the tensor correlation length ξ_T defined in the $2N$-vector model.

Analogous relations hold for the Binder parameter. As in the O(n) case, we consider two additional Binder parameters

$$U_3 = \frac{\langle \text{Tr}\, \Theta_{\text{CP}}^3 \rangle}{\langle \text{Tr}\, \Theta_{\text{CP}}^2 \rangle^{3/2}}, \quad U_b = \frac{\langle \text{Tr}\, \Theta_{\text{CP}}^4 \rangle}{\langle \text{Tr}\, \Theta_{\text{CP}}^2 \rangle^2}. \tag{B6}$$

where

$$\Theta_{\text{CP}}^{ab} = \sum_x Q_x^{ab}. \tag{B7}$$

For $N = 2$, we have $U_{3\text{CP}} = 0$ and $U = 2U_b$.

In the high-temperature phase we have $U_3 = 0$,

$$U = \frac{N^2+1}{N^2-1}, \quad U_b = \frac{2N^2-3}{N(N^2-1)}. \tag{B8}$$

TABLE II. We report some numerical values of the scaling functions $F(x)$ that give the values of the Binder parameters and of ξ_V/ξ_T as a function of $x = \xi_T/L$; see Eq. (25). Results in the scaling limit for $n = 3, 4, 5, 8$. If the function has a maximum, in the second and third column we report the position $x_{\max}$ of the maximum and Max $= F(x_{\max})$. In the last five columns we report $F(x)$ for $x = 0.1, 0.2, 0.3, 0.4, 0.5$.

n	$x_{\max}$	Max	$x = 0.1$	$x = 0.2$	$x = 0.3$	$x = 0.4$	$x = 0.5$
				U_{3T}			
3			0.162(4)	0.325(8)	0.372(2)	0.390(2)	0.398(1)
4			0.212(1)	0.422(8)	0.517(2)	0.548(2)	0.561(1)
5			0.246(7)	0.502(7)	0.597(3)	0.634(2)	0.654(1)
8			0.268(1)	0.576(3)	0.703(2)	0.753(1)	0.775(1)
				$U_{4T,a}$			
3	0.132(2)	1.60(3)	1.57(3)	1.49(2)	1.261(2)	1.146(5)	1.080(1)
4	0.141(2)	1.39(2)	1.336(5)	1.317(2)	1.178(4)	1.099(2)	1.054(1)
5	0.155(1)	1.29(1)	1.250(7)	1.256(2)	1.144(4)	1.075(2)	1.041(1)
8	0.154(1)	1.17(1)	1.1269(3)	1.142(2)	1.089(3)	1.044(1)	1.0239(4)
				$U_{4T,b}$			
3	0.132(2)	0.80(2)	0.78(2)	0.745(1)	0.631(1)	0.573(2)	0.540(1)
4	0.205(1)	0.692(6)	0.626(3)	0.685(3)	0.649(2)	0.622(2)	0.604(1)
5	0.25(4)	0.68(1)	0.549(7)	0.679(9)	0.678(4)	0.665(2)	0.658(1)
8			0.407(1)	0.644(3)	0.721(2)	0.746(1)	0.7562(2)
				ξ_V/ξ_T			
3			3.37(5)	2.71(2)	2.46(1))	2.296(8)	2.171(8)
4			3.23(5)	2.62(3)	2.30(1)	2.125(4)	2.008(7)
5			3.18(2)	2.49(2)	2.20(1)	2.029(3)	1.918(6)
8			3.01(2)	2.34(1)	2.05(1)	1.893(3)	1.788(4)

In the low-temperature phase we have $U = 1$,

$$U_3 = \frac{N-2}{\sqrt{N(N-1)}}, \tag{B9}$$

$$U_b = \frac{N^2-3N+3}{N(N-1)}. \tag{B10}$$

To compute the scaling functions associated with these quantities in the O($2N$) theory, we use the mapping (B3). It is easy to verify that

$$\Theta^{ab}_{\rm CP} = \Theta^{ab} + \Theta^{a+N,b+N} + i\Theta^{a,b+N} - i\Theta^{a+N,b}. \tag{B11}$$

Squaring the previous relation and taking the trace, we obtain

$$\mathrm{Tr}\,\Theta^2_{\rm CP} = \mathrm{Tr}\,\Theta^2 + \sum_{a,b=1}^{N} (\Theta^{ab}\Theta^{a+N,b+N} - \Theta^{a,b+N}\Theta^{a+N,b}). \tag{B12}$$

In this relation, the trace in the l.h.s. is performed in the CP^{N-1} theory (indices go from 1 to N), while the trace in the r.h.s. is performed in the O($2N$) theory (indices go from 1 to $2N$). The presence of the additional terms in Eq. (B12) explains why the relation between the CP^{N-1} Binder parameters and the tensor Binder parameters in the O($2N$) theory is not trivial.

Using the O($2N$) invariance of the model we obtain the relations

$$\langle \mathrm{Tr}\,\Theta^2_{\rm CP}\rangle = \frac{2(N-1)}{2N-1}\langle \mathrm{Tr}\,\Theta^2\rangle,$$

$$\langle \mathrm{Tr}\,\Theta^3_{\rm CP}\rangle = \frac{2(N-2)}{2N-1}\langle \mathrm{Tr}\,\Theta^3\rangle,$$

$$\langle [\mathrm{Tr}\,\Theta^2_{\rm CP}]^2\rangle = \frac{4N}{(2N-3)(4N^2-1)} \times [(2N^2-5N+4)(\langle [\mathrm{Tr}\,\Theta^2]^2\rangle - 2\langle \mathrm{Tr}\,\Theta^4\rangle],$$

$$\langle \mathrm{Tr}\,\Theta^4_{\rm CP}\rangle = \frac{2}{(2N-3)(4N^2-1)} \times [(4N^2-3N-6)\langle [\mathrm{Tr}\,\Theta^2]^2\rangle + 2(2N^3-9N^2+6N+6)\langle \mathrm{Tr}\,\Theta^4\rangle]. \tag{B13}$$

We obtain therefore the relations, which are exact for the O($2N$) theory, between CP^{N-1} and tensor O($2N$) Binder parameters defined in Appendix A:

$$U_3 = \frac{N-2}{N-1}\sqrt{\frac{2N-1}{2(N-1)}}\,U_{3T},$$

$$U = \frac{N(2N-1)}{(N-1)^2(2N+1)(2N-3)} \times [(2N^2-5N+4)U_{4T,a} - 2U_{4T,b}],$$

$$U_b = \frac{2N-1}{2(N-1)^2(2N+1)(2N-3)} \times [(4N^2-3N-6)U_{4T,a} + 2(2N^3-9N^2+6N+6)U_{4T,b}]. \tag{B14}$$

For $N = 2$ and $N = 4$, the two cases of relevance in this work, we obtain

$$U = \tfrac{12}{5}(U_{4T,a} - U_{4T,b}),$$

$$U = \tfrac{448}{405}U_{4T,a} - \tfrac{56}{405}U_{4T,b}, \tag{B15}$$

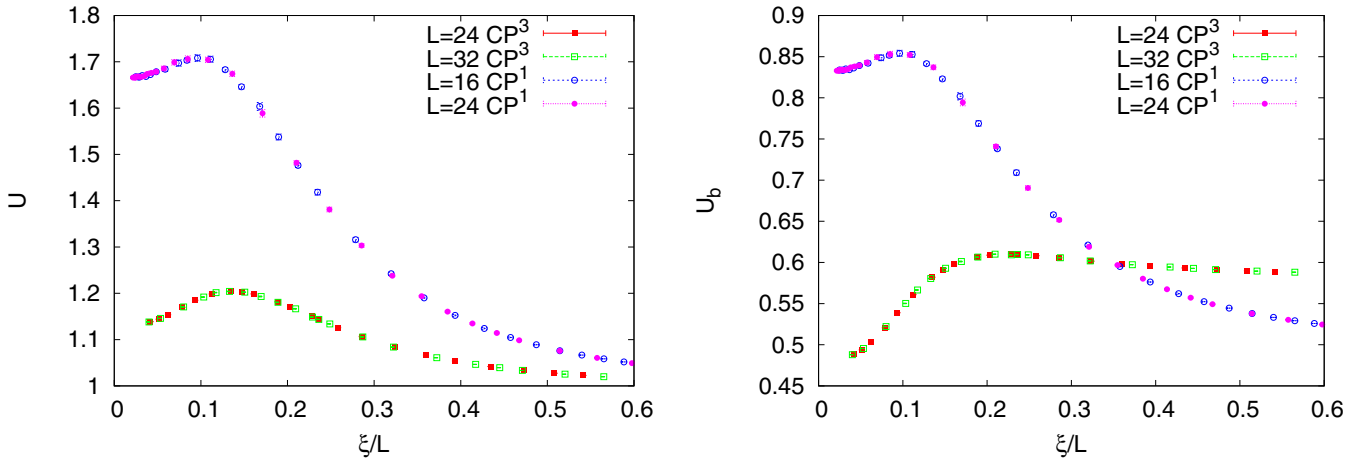

FIG. 13. Scaling functions of the CP^{N-1} Binder parameters in the O($2N$) model, computed using O($2N$) tensor data and Eq. (B14). For $N = 2$ we have $U_b = U/2$. For $\xi_T/L \to 0$, we have $U \approx 1.667$, $U_b \approx 0.833$ for $N = 2$, and $U \approx 1.133$, $U_b \approx 0.483$ for $N = 4$. In the limit $\xi_T/L \to \infty$, $U = 1$ for any N and and $U_b = 0.5, 0.583$ for $N = 2, 4$, respectively.

respectively. To obtain the scaling functions associated with the CP^{N-1} Binder parameters in the large-β_g limit, we have therefore performed simulations in the n-vector model with $n = 2N$, we have computed the tensor Binder parameters $U_{4T,a}$ and $U_{4T,b}$, and we have applied Eq. (B15). Results are reported in Fig. 13.

[1] J. Smiseth, E. Smørgrav, F. S. Nogueira, J. Hove, and A. Sudbø, Phase structure of $d = 2 + 1$ compact lattice gauge theories and the transition from mott insulator to fractionalized insulator, Phys. Rev. B **67**, 205104 (2003).

[2] J. Smiseth, E. Smorgrav, and A. Sudbø, Critical Properties of the N-Color London Model, Phys. Rev. Lett. **93**, 077002 (2004).

[3] E. Babaev, A. Sudbø, and N. W. Ashcroft, A superconductor to superfluid phase transition in liquid metallic hydrogen, Nature (London) **431**, 666 (2004).

[4] O. I. Motrunich and A. Vishwanath, Emergent photons and transitions in the O(3) sigma model with hedgehog suppression, Phys. Rev. B **70**, 075104 (2004).

[5] T. Senthil, L. Balents, S. Sachdev, A. Vishwanath, and M. P. A. Fisher, Quantum criticality beyond the Landau-Ginzburg-Wilson paradigm, Phys. Rev. B **70**, 144407 (2004).

[6] K. Kataoka, S. Hattori, and I. Ichinose, Effective field theory for Sp(N) antiferromagnets and their phase structure, Phys. Rev. B **83**, 174449 (2011)

[7] B. I. Halperin, T. C. Lubensky, and S. K. Ma, First-Order Phase Transitions in Superconductors and Smectic-A Liquid Crystals, Phys. Rev. Lett. **32**, 292 (1974).

[8] M. Moshe and J. Zinn-Justin, Quantum field theory in the large N limit: A review, Phys. Rep. **385**, 69 (2003).

[9] K. Kajantie, M. Karjalainen, M. Laine, and J. Peisa, Masses and phase structure in the Ginzburg-Landau model, Phys. Rev. B **57**, 3011 (1998).

[10] H. Kleinert, F. S. Nogueira, and A. Sudbø, Deconfinement Transition in Three-Dimensional Compact U(1) Gauge Theories Coupled to Matter Fields, Phys. Rev. Lett. **88**, 232001 (2002).

[11] S. Mo, J. Hove, and A. Sudbø, Order of the metal-to-superconductor transition, Phys. Rev. B **65**, 104501 (2002).

[12] S. Wenzel, E. Bittner, W. Janke, A. M. J. Schakel, and A. Schiller, Kertesz Line in the Three-Dimensional Compact U(1) Lattice Higgs Model, Phys. Rev. Lett. **95**, 051601 (2005).

[13] M. N. Chernodub, E. M. Ilgenfritz, and A. Schiller, Phase structure of an Abelian two-Higgs model and high-temperature superconductors, Phys. Rev. B **73**, 100506(R) (2006).

[14] Note that our coupling β_g differs by a factor of 2 from the one used in other works. If $\lambda_{\boldsymbol{x},\mu} = \exp(i\theta_{\boldsymbol{x},\mu})$, the gauge part of the Hamiltonian reads $H_{\text{gauge}} = -2\beta_g \cos\theta_{\boldsymbol{x},\mu\nu}$, with $\theta_{\boldsymbol{x},\mu\nu} = \theta_{\boldsymbol{x},\mu} - \theta_{\boldsymbol{x}+\hat{\nu},\mu} - \theta_{\boldsymbol{x},\nu} + \theta_{\boldsymbol{x}+\hat{\mu},\nu}$.

[15] A. Pelissetto and E. Vicari, Three-dimensional ferromagnetic CP^{N-1} models, Phys. Rev. E **100**, 022122 (2019).

[16] A. Nahum, J. T. Chalker, P. Serna, M. Ortuño, and A. M. Somoza, 3D Loop Models and the CP^{N-1} Sigma Model, Phys. Rev. Lett. **107**, 110601 (2011).

[17] A. Nahum, J. T. Chalker, P. Serna, M. Ortuño, and A. M. Somoza, Phase transitions in three-dimensional loop models and the CP^{N-1} sigma model, Phys. Rev. B **88**, 134411 (2013).

[18] F. Delfino, A. Pelissetto, and E. Vicari, Three-dimensional antiferromagnetic CP^{N-1} models, Phys. Rev. E **91**, 052109 (2015).

[19] A. Pelissetto, A. Tripodo, and E. Vicari, Landau-Ginzburg-Wilson approach to critical phenomena in the presence of gauge symmetries, Phys. Rev. D **96**, 034505 (2017).

[20] A. Pelissetto and E. Vicari, Critical phenomena and renormalization group theory, Phys. Rep. **368**, 549 (2002).

[21] T. Ono, S. Doi, Y. Hori, I. Ichinose, and T. Matsui, Phase structure and critical behavior of multi-higgs U(1) lattice gauge theory in three dimensions, Ann. Phys. (NY) **324**, 2453 (2009).

[22] S. Takashima, I. Ichinose, and T. Matsui, CP^1+U(1) lattice gauge theory in three dimensions: Phase structure, spins, gauge bosons, and instantons, Phys. Rev. B **72**, 075112 (2005).

[23] In Refs. [6,21,22], the system sizes were quite small and the data had a limited precision, preventing the authors to obtain a satisfactory understanding of the nature of the transitions and of the crossover behaviors along the transition lines.

[24] A. Polyakov, Compact gauge fields and the infrared catastrophe, Phys. Lett. B **59**, 82 (1975); for an extensive list of references, see A. Athenodorou and M. Teper, On the spectrum and string tension of U(1) lattice gauge theory in $2+1$ dimensions, J. High Energy Phys. 01 (2019) 063; M. Caselle, A. Nada, M. Panero, and D. Vadacchino, Conformal field theory and the hot phase of three-dimensional $U(1)$ gauge theory, *ibid.* 05 (2019) 068.

[25] B. Ihrig, N. Zerf, P. Marquard, I. F. Herbut, and M. M. Scherer, Abelian Higgs model at four loops, fixed-point collision, and deconfined criticality, Phys. Rev. B **100**, 134507 (2019).

[26] R. Folk and Y. Holovatch, On the critical fluctuations in superconductors, J. Phys. A **29**, 3409 (1996).

[27] G. Fejos and T. Hatsuda, Renormalization group flows of the N-component Abelian Higgs model, Phys. Rev. D **96**, 056018 (2017).

[28] L. D. Landau and E. M. Lifshitz, *Statistical Physics. Part I*, 3rd ed. (Elsevier Butterworth-Heinemann, Oxford, 1980).

[29] K. G. Wilson and J. Kogut, The renormalization group and the ϵ expansion, Phys. Rep. **12**, 75 (1974).

[30] M. E. Fisher, The renormalization group in the theory of critical behavior, Rev. Mod. Phys. **47**, 543 (1975).

[31] S.-K. Ma, *Modern Theory of Critical Phenomena* (W. A. Benjamin, Reading, MA, 1976).

[32] A. Pelissetto, A. Tripodo, and E. Vicari, Criticality of O(N) symmetric models in the presence of discrete gauge symmetries, Phys. Rev. E **97**, 012123 (2018).

[33] P. Calabrese, P. Parruccini, A. Pelissetto, and E. Vicari, Critical behavior of O(2) $\otimes$ O(N)-symmetric models, Phys. Rev. B **70**, 174439 (2004).

[34] Y. Nakayama and T. Ohtsuki, Approaching the conformal window of $O(n)\times O(m)$ symmetric Landau-Ginzburg models using the conformal bootstrap, Phys. Rev. D **89**, 126009 (2014); Bootstrapping phase transitions in QCD and frustrated spin systems, **91**, 021901(R) (2015).

[35] M. De Prato, A. Pelissetto, and E. Vicari, Normal-to-planar superfluid transition in ^{3}He, Phys. Rev. B **70**, 214519 (2004).

[36] M. Campostrini, P. Rossi, and E. Vicari, Monte Carlo simulation of CP^{N-1} models, Phys. Rev. D **46**, 2647 (1992).

[37] L. Del Debbio, G. Manca, and E. Vicari, Critical slowing down of topological modes, Phys. Lett. B **594**, 315 (2004).

[38] M. Hasenbusch, Fighting topological freezing in the two-dimensional CP^{N-1} model, Phys. Rev. D **96**, 054504 (2017).

[39] V. Alba, A. Pelissetto, and E. Vicari, The uniformly frustrated two-dimensional XY model in the limit of weak frustration, J. Phys. A: Math. Theor. **41**, 175001 (2008).

[40] H. G. Ballesteros, L. A. Fernandez, V. Martin-Mayor, and A. Munoz Sudupe, Finite size effects on measures of critical exponents in $d=3$ O(N) models, Phys. Lett. B **387**, 125 (1996).

[41] M. Campostrini, A. Pelissetto, P. Rossi, and E. Vicari, Four-point renormalized coupling in O(N) models, Nucl. Phys. B **459**, 207 (1996).

[42] M. Hasenbusch and E. Vicari, Anisotropic perturbations in 3D O(N) vector models, Phys. Rev. B **84**, 125136 (2011).

[43] M. Campostrini, M. Hasenbusch, A. Pelissetto, P. Rossi, and E. Vicari, Critical exponents and equation of state of the three-dimensional Heisenberg universality class, Phys. Rev. B **65**, 144520 (2002).

[44] R. Guida and J. Zinn-Justin, Critical exponents of the N-vector model, J. Phys. A **31**, 8103 (1998).

[45] M. S. S. Challa, D. P. Landau, and K. Binder, Finite-size effects at temperature-driven first-order transitions, Phys. Rev. B **34**, 1841 (1986).

[46] K. Vollmayr, J. D. Reger, M. Scheucher, and K. Binder, Finite size effects at thermally-driven first order phase transitions: A phenomenological theory of the order parameter distribution, Z. Phys. B **91**, 113 (1993).

[47] R. D. Pisarski and F. Wilczek, Remarks on the chiral phase transition in chromodynamics, Phys. Rev. D **29**, 338 (1984).

[48] A. Butti, A. Pelissetto, and E. Vicari, On the nature of the finite-temperature transition in QCD, J. High Energy Phys. 08 (2003) 029.

[49] A. Pelissetto and E. Vicari, Relevance of the axial anomaly at the finite-temperature chiral transition in QCD, Phys. Rev. D **88**, 105018 (2013).

[50] T. Senthil, A. Vishwanath, L. Balents, S. Sachdev, and M. P. A. Fisher, Deconfined quantum critical points, Science **303**, 1490 (2004).

[51] T. Senthil, L. Balents, S. Sachdev, A. Vishwanath, and M. P. A. Fisher, Deconfined criticality critically defined, J. Phys. Soc. Jpn. **74**, 1 (2005).

[52] M. A. Metliski, M. Harmele, T. Senthil, and M. P. A. Fisher, Monopoles in CP^{N-1} model via the state-operator correspondence, Phys. Rev. B **78**, 214418 (2008).

[53] M. S. Block, R. G. Melko, and R. K. Kaul, Fate of $\mathbb{C}P^{N-1}$ Fixed Points with q Monopoles, Phys. Rev. Lett. **111**, 137202 (2013).

[54] G. J. Sreejith and S. Powell, Scaling dimensions of higher-charge monopoles at deconfined critical points, Phys. Rev. B **92**, 184413 (2015).

[55] E. Dyer, M. Mezei, S. S. Pufu, and S. Sachdev, Scaling dimensions of monopole operators in the $\mathbb{C}P^{N_b-1}$ theory in $2+1$ dimensions, J. High Energy Phys. 6 (2015) 037.

[56] A. B. Kuklov, M. Matsumoto, N. V. Prokof'ev, B. V. Svistunov, and M. Troyer, Deconfined Criticality: Generic First-Order Transition in the SU(2) Symmetry Case, Phys. Rev. Lett. **101**, 050405 (2008).

[57] A. Nahum, J. T. Chalker, P. Serna, M. Ortuño, and A. M. Somoza, Deconfined Quantum Criticality, Scaling Violations, and Classical Loop Models, Phys. Rev. X **5**, 041048 (2015).

[58] P. Butera and M. Comi, N-vector spin models on the simple-cubic and the body-centered-cubic lattices: A study of the critical behavior of the susceptibility and of the correlation length by high-temperature series extended to order β^{21}, Phys. Rev. B **56**, 8212 (1997).

[59] M. Hasenbusch, Eliminating leading corrections to scaling in the three-dimensional O(N)-symmetric ϕ^4 model: $N=3$ and 4, J. Phys. A **34**, 8221 (2001).

[60] M. Hasenbusch, A. Pelissetto, and E. Vicari, Instability of O(5) multicritical behavior in SO(5) theory of high-T_c superconductors, Phys. Rev. B **72**, 014532 (2005).